การสังเคราะห์อนุภาคคาร์บอนในระดับนาโนเมตรโดยอาศัยการไพโรไรซิสของผสมระหว่างเฟอโรซีนและแนฟทาลีน

นายปราโมทย์ ผึ้งจินดา

วิทยานิพนธ์นี้เป็นส่วนหนึ่งของการศึกษาตามหลักสูตรปริญญาวิศวกรรมศาสตรมหาบัณฑิต
สาขาวิชาวิศวกรรมเคมี ภาควิชาวิศวกรรมเคมี
คณะวิศวกรรมศาสตร์ จุฬาลงกรณ์มหาวิทยาลัย
ปีการศึกษา 2547
ISBN 974-53-1260-6

SYNTHESIS OF CARBON NANOPARTICLES USING PYROLYSIS OF FERROCENE-NAPHTHALENE MIXTURE

Mr. Pramote Puengjinda

A Thesis Submitted in Partial Fulfillment of the Requirements
for the Degree of Master of Engineering in Chemical Engineering
Department of Chemical Engineering
Faculty of Engineering
Chulalongkorn University
Academic Year 2004

ISBN 974-53-1260-6

Thesis Title	SYNTHESIS OF CARBON NANOPARTICLES USING PYROLYSIS OF FERROCENE-NAPHTHALENE MIXTURE
By	Mr. Pramote Puengjinda
Field of study	Chemical Engineering
Thesis Advisor	Associate Professor Tawatchai Charinpanitkul, D.Eng.
Thesis Co-advisor	Professor Wiwut Tanthapanichakoon, Ph.D.

Accepted by the Faculty of Engineering, Chulalongkorn University in Partial Fulfillment of the Requirements for the Master's Degree

…..……Dean of the Faculty of Engineering
(Professor Direk Lavansiri, Ph.D.)

THESIS COMMITTEE

……..Chairman
(Associate Professor Suttichai Assabumrungrat, Ph.D.)

……...Thesis Advisor
(Associate Professor Tawatchai Charinpanitkul, D.Eng.)

……Thesis Co-advisor
(Professor Wiwut Tanthapanichakoon, Ph.D.)

……...Member
(Chanchana Thanachayanont, Ph.D)

……..Member
(Varong Pavarajarn, Ph.D.)

ปราโมทย์ ผึ้งจินดา : การสังเคราะห์อนุภาคคาร์บอนในระดับนาโนเมตรโดยอาศัยการไพโรไรซิสของผสมระหว่างเฟอโรซีนและแนฟทาลีน (SYNTHESIS OF CARBON NANOPARTICLE USING PYROLYSIS OF FERROCENE-NAPHTHALENE MIXTURE) อ. ที่ปรึกษา: รศ.ดร .ธวัชชัย ชรินพาณิชกุล, อ.ที่ปรึกษาร่วม: ศ.ดร .วิวัฒน์ ตัณฑะพานิชกุล, จำนวนหน้า 97 หน้า. ISBN 974-53-1260-6

การไพโรไลซิสร่วมของของผสมระหว่างเฟอโรซีนและแนฟทาลีนสามารถสังเคราะห์อนุภาคคาร์บอนในระดับนาโนเมตรที่มีโลหะเหล็กเป็นองค์ประกอบภายในชั้นของแกรไฟต์ โดยอนุภาคที่สังเคราะห์ได้นั้นประกอบด้วยอนุภาคสองประเภทใหญ่ๆคือ ท่อนาโนคาร์บอน และคาร์บอนนาโนแคปซูล จุดเด่นของงานวิจัยนี้คือการใช้แนฟทาลีนเป็นแหล่งคาร์บอนเพิ่มเติมในการสังเคราะห์เพื่อลดปริมาณการใช้เฟอโรซีนลงซึ่งนับว่าเป็นวิธีการลดค่าใช้จ่ายในการลงทุนได้อีกวิธีหนึ่ง

ในงานวิจัยนี้ได้ทำการศึกษาถึงอิทธิพลอุณหภูมิที่ใช้ในการไพโรไลซิส, อัตราส่วนผสมของของผสม ,อัตราการไหลและชนิดของแก๊สต่อลักษณะของอนุภาคที่สังเคราะห์ได้ ซึ่งจากผลการทดลองพบว่าอุณหภูมิในช่วง 800-1050°C นั้นมีอิทธิพลอย่างมากต่อการเกิดอนุภาคเหล่านี้โดยที่อุณหภูมิสูงอนุภาคของเหล็กจะมีความว่องไวในการเกิดปฏิกิริยาสูงทำให้สามารถเกิดเป็นคาร์บอนนาโนแคปซูลได้รวดเร็วอีกทั้งที่อุณหภูมิสูงจะเกิดการรวมตัวของอนุภาคเหล็กทำให้อนุภาคที่ได้มีขนาดใหญ่ ในทางกลับกันที่อุณหภูมิต่ำคาร์บอนอิสระจะเรียงตัวต่อกันอย่างเป็นระเบียบเนื่องจากอัตราการแพร่ของคาร์บอนอิสระเป็นตัวควบคุมการเกิดปฏิกิริยาทำให้เกิดเป็นท่อนาโนคาร์บอนที่เรียงตัวเป็นระเบียบได้

การเพิ่มปริมาณคาร์บอนของอิสระขึ้น จะทำให้ได้สัดส่วนของคาร์บอนอิสระต่อตัวเร่งปฏิกิริยาสูงขึ้นโดยอนุภาคที่สังเคราะห์ได้มีลักษณะเป็นท่อนาโนคาร์บอนมากกว่าคาร์บอนนาโนแคปซูล ส่วนชนิดของแก๊สที่ใช้ในกระบวนการนั้นจะส่งผลต่ออนุภาคที่สังเคราะห์ได้โดยเมื่อสังเคราะห์ภายใต้บรรยากาศของไนโตรเจนนั้นอนุภาคที่ได้นั้นจะมีสัดส่วนของปริมาณคาร์บอนอสัณฐาน(amorphous carbon) สูงกว่าอนุภาคทั้งสองแบบนี้แต่เมื่อเปลี่ยนเป็นบรรยากาศของอาร์กอนจะช่วยลดสัดส่วนของ คาร์บอนอสัณฐานลงโดยบทบาทของแก๊สอาร์กอนนั้นช่วยทำให้ลดการเกิดออกซิเดชันของอนุภาคเหล็กที่เกิดขึ้นและช่วยเสริมการฟอร์มชั้นแกรไฟต์ของคาร์บอนได้ดีกว่าแก๊สไนโตรเจน

ภาควิชา.....วิศวกรรมเคมี.....ลายมือชื่อนิสิต.....
สาขาวิชา.....วิศวกรรมเคมี.....ลายมือชื่ออาจารย์ที่ปรึกษา.....
ปีการศึกษา.....2547……ลายมือชื่ออาจารย์ที่ปรึกษาร่วม.....

4670372621 : MAJOR CHEMICAL ENGINEERING
KEY WORD: CARBON NANOTUBES / CARBON NANOCAPSULES / PYROLYSIS
PRAMOTE PUENGJINDA : THESIS TITLE. (SYNTHESIS OF CARBON NANOPARTICLE USING PYROLYSIS OF FERROCENE-NAPHTHALENE MIXTURE) THESIS ADVISOR: ASSOC. PROF. TAWATCHAI CHARINPANITKUL, D.Eng., THESIS COADVISOR : PROF. WIWUT TANTHAPANICHAKOON, Ph.D., 97 pp. ISBN 974-53-1260-6

Thermal co-pyrolysis of ferrocene and naphthalene mixture has been successfully developed to synthesize carbon nanoparticles (CNPs). The synthesized products are composed of 2 types of carbon nanoparticles namely, carbon nanotubes (CNTs) and carbon nanocapsules (CNCs). The distinctive point of this work is to use naphthalene as an additional carbon source for synthesize CNTs, which could help reduce quatity of ferrocene, resulting in lower operating cost of synthesis.

In this research the effects of pyrolysis temperature, molar ratio of mixture, type of carrier gas and carrier gas flow rate on characteries of the obtained nanoparticles are comprehensively investigated. Based on experimental results, the pyrolysis temperature with average of 800-1050˚C provides significant influence on the morphology of the synthesized nanoparticles. CNCs are preferable to form at high. On the other hand, well-aligned CNTs become predominant products at lower pyrolysis temperature because diffusion of free carbon might play a controlling role.

An increase in fraction of naphthalene, which could reach to higher ratio of carbon atoms to iron catalyst atoms, could give rise to high CNTs formation. Interestingly, when Argon is employed as carrier gas it could provide crystalline products of CNCs and CNTs quantity higher than using Nitrogen. This is attributable to the lower reactive characteristics of Argon compared to Nitrogen.

Department..Chemical Engineering.....Student's signature.....

Field of study.....Chemical Engineering……..Advisor's signature.....

Academic year ……..2004.....CO-advisor's signature.....

ACKNOWLEDGEMENTS

I am very grateful to my advisor, Assoc. Prof. Tawatchai Charinpanitkul, Department of Chemical Engineering, Chulalongkorn University, for his indispensable advice, and his encouragement to continue the course of this work. I am also grateful to my co-advisor, Prof. and Assoc. Prof. Sutthichai Assabumrungrut, Dr. Varong Pavarajarn, Dr. Chanchana Thanachayanont for their stimulative comments and participation as the thesis committee.

I would like to acknowledge Dr. Sano, Hyogo University Japan, for his useful guidance, comments, research assistance, and kindness. It has been a great experience learning a lot of things from him.

The research work received research grant from the Thailand Research Fund (TRF-RTA of Prof. Wiwut Tanthapanichakoon and TRF-MAG) for financial support. The Project is headed by Assoc. Prof. Tawatchai Charinpanitkul and I am one of the half-time research assistants.

I would like to thank my senior colleagues, Mr. Poonlasak Muthakarn, for his useful suggestions and analytical data from him. I would like to thank the officers from National Metal and Materials Technology Center (MTEC), TEM analytical room, for their suggestion and information on the analytical instrument.

I would like to thank the Department of Chemical Engineering, Chulalongkorn University for allowing me to setup the experimental apparatus and using the accessories.

Thank you very much to all members of the Particle Technology and Material Processing Laboratory for their warm collaborations and kindness during my thesis work.

Finally it is my great wish to express my cordial and deep thanks to my parents for their love and encouragement.

CONTENTS

CONTENTS (CONTINUED)

CONTENTS (CONTINUED)

LIST OF TABLES

LIST OF FIGURES

Page

LIST OF FIGURES

LIST OF FIGURES

LIST OF FIGURES

NOMENCLATURES

MWNTs	Multi-walled carbon nanotubes
SWNTs	Single-walled carbon nanotubes
CNPs	Carbon nanoparticles
CNTs	Carbon nanotubes
CNCs	Carbon nanocapsules
SEM	Scanning Electron Microscope
TEM	Transmission Electron Microscope
XRD	X-ray diffraction
HRTEM	High Resolution Transmission Electron Microscope
DLS	Dynamic Light Scattering
EDX	Energy Dispersive X-ray
RBM	Radial Breathing Mode
CVD	Chemical Vapor Deposition
d	Single-walled carbon nanotubes diameter(nm)
ω	Radial Breathing Mode frequency (cm^{-1})
ρ	Density of gas ($kg\ m^{-3}$)
μ	Viscosity of gas ($Pa \cdot s$)
ν	Superficial velocity ($m\ s^{-1}$)
υ	Space time (min)
V	Volume of the reactor (m^3)

CHAPTER I

INTRODUCTION

1.1 Introduction

Discovery of carbon nanotubes by Iijima in 1991 [1] has initiated substantial attentions in many research areas, particularly those of synthesizing carbon nanoparticles (CNPs), such as nanotubes, nanohorns, nanocapsules and so on [2-7]. Among these novel materials, carbon nanotube is more attractive than the others because of its unique structure and extraordinary physical properties which are expected for many promising applications including field emission display [9], atomic force microscopy (AFM) tips, hydrogen storage, electronics devices and so on. Not only carbon nanotubes have many various applications but carbon nanocapsules also become interesting nanomaterials due to their structures which carbon shells can immunize the encapsulated species to avoid environmental degradation effects while retaining their intrinsic properties [18,20] which are expect for magnetic recording media, magnetic toner and so on [21,25]. So far, besides the laser ablation method which is originally proposed by Iijima, many other methods including standard and modified, i.e., plasma-enhanced chemical vapor deposition (PECVD), arc discharge [2] and thermal pyrolysis of organometallic compounds have been applied for CNPs synthesis [5-14].

Among those methodologies, thermal pyrolysis is seemed to be efficient for large-scale carbon nanoparticles production coexistingly with low operating costs. Many reports have revealed that thermal pyrolysis of ferrocene can be employed for synthesizing carbon nanotubes and nanocapsules with Fe atoms in carbon shell [14]. However, using additional carbon sources, i.e., *p*-xylene, benzene [12,16] and anthracene [15], acetylene [8,9,13,23] mixed with ferrocene, can either provide more carbon nanoparticles or decrease the amount of ferrocene used.

It is noteworthy that naphthalene is known as one of good alternatives for carbon source because of its abundance and similarity in chemical structure compared with ferrocene. Therefore, a mixture of ferrocene and naphthalene could be expected

as raw materials for thermal co-pyrolysis to provide carbon nanoparticles. However, there are very limited reports on the co-pyrolysis of such mixture. This work sets its aims to investigate the possibility in employing co-pyrolysis of ferrocene-naphthalene mixtures to synthesize CNPs. Then some experimental parameters such as pyrolysis temperature, mole ratio of the mixtures, carrier gas flow rate will be varied to find out the optimal conditions.

1.2 Objectives

The main objectives of this research work is to set up a co-pyrolysis equipment and conduct experiments for producing nanoparticles using ferrocene and naphthalene mixture and then investigate the effect of pyrolysis temperature, types of carrier gas, mass ratio of ferrocene to naphthalene and flow rate of carrier gas on the structure and yield of carbon nanoparticles.

1.3 Scope of research works

The scope of this research is limited in laboratory scale as follows:

1. Design and construct the experimental apparatus for co-pyrolysis tasks.
2. Study the effect of pyrolysis temperature in the range of 800-1100 °C
3. Study the effect of carrier gas flow rate in the range of 50-100 cm^3/min
4. Study the effect of type of carrier gas
   4.1 Species of carrier gas to be investigated
   - Argon - Nitrogen
5. Study the ratio of mixture of ferrocene and naphthalene
   5.1 The molar ratio of ferrocene to naphthalene to be investigated are
   - 1:1 - 1:2 - 1:5
6. Characterize obtained nanoparticles using SEM (Scanning Electron Microscopy), TEM (Transmission Electron Microscopy), DLS (Dynamic Light Scattering) and Raman Spectroscopy

1.4 Procedure of the research

1. Explore and review literature related to the research
2. Design and construct the experimental setup
3. Conduct experiments to repeat the conventional method of nanoparticles-synthesis
4. Conduct experiments by varying pyrolysis temperature, carrier gas flow rate, type of carrier gas and the molar ratio of the mixture
5. Study and estimate properties of the obtained nanoparticles
6. Discuss experimental results
7. Draw conclusion
8. Write the thesis

1.5 Expected benefits

1. Gain knowledge of pyrolysis technique for synthesizing carbon nanoparticles
2. Understand the effect of temperature and other operating parameters on the characteristics and yield of carbon nanoparticles to be obtained.
3. Understand the preliminary information of the formation mechanism of carbon nanoparticles within the proposed system

CHAPTER II

LITERATURE REVIEW

This chapter will notify some review of representative reports involving carbon nanoparticles synthesis by various methodologies. However, thermal pyrolysis technique will be more emphasized here. Several reports have been made use of pure ferrocene or ferrocene solution (in benzene, toluene,etc.) as carbon source and argon or hydrogen as carrier gas pyrolysis. Those previous investigationa are the initiation of this work. They are summarized as follows,

2.1 Methodologies for carbon nanoparticles synthesis

N. Sano et al. (2004) investigated the effect of force convection jet on the arc plasma to synthesize CNPs such as MW-CNTs and multi-shelled nanoparticles by arc discharge in water method. They found that there is an optimized flow rate of the convective jet that leads to the highest yield, largest hydrodynamic diameter of the products, and the reduced crystalline defects. With the convection flow rate of 1.36 dm^3 /min, the highest yield and production rate of CNPs could be obtained at 48.5% and 9.32 g/h, respectively [2].

Y. Kobayashi et al. (2004) investigated single-walled carbon nanotube (SWNT) growth using a novel Fe_3O_4 nanoparticle catalyst synthesized with a simple organic chemistry process. Discrete nanoparticles with a uniform diameter of ~4 nm could be deposited on Si substrates with a thermal oxide layer by spin-coating with a nanoparticle solution. These nanoparticles were found to have remarkable catalytic activity in the CVD growth of the SWNTs. SWNTs with diameters of around 1 nm were produced from the reduced nanoparticle catalyst. The diameters of the grown SWNTs were closely correlated with those of the catalytic nanoparticles and tended to be slightly smaller than the particle size [3].

M. Zhang et al. (2001) were able to increase the percentage of SWNTs and decrease impurities in the form of graphite particles and amorphous carbon by using a new target. The new target materials was made of crude SWNTs, which contained SWNTs (20-30%), particles of graphite(10-20%), amorphous carbon (50-60%) and a little of Co and Ni (about 0.6%). SWNTs were formed by laser ablation using quartz-glass tube chamber under 600-750 torr at temperature 1200°C.The surface of taget irradiated by a pulsed Nd-YAG laser beam (wave length; 532 nm and frequency 10 Hz) for 1 min [4].

2.2 Pyrolysis method enhanced with catalyst film on substrate

W.D. Zhang et al. (2002) found that using a common chemical, ethylenediamine, without being plasma aided, could successfully provide vertically aligned bamboo-like multi-walled CNTs on Ni-deposited silicon wafers with high density by CVD. The diameter of CNTs ranges from 100 to 150 nm and the length can be controlled from 10 to 50 mm by varying the CVD time from 5 to 40 min [5].

H.Ago et al. (2005) has used a vertical flow reactor for synthesizing single and multi-walled carbon nanotubes by the gas-phase catalytic reaction of colloidal solutions of metal nanoparticles. They used reverse micelle solution of the Co–Mo nanoparticles dissolved in toluene as raw materials and injected directly into the reactor maintained at 1200°C. The growth of SWNTs was observed when the small amount of thiophene was added in the colloidal solution (1 wt. %). However, when they added 10 wt. % of thiophene, only MWNTs can be grown from the gas-phase reaction. Carbon nanotubes received have a metal nanoparticle encapsulated at the tip [6].

C. Emmenegger et al. (2002) have grown carbon nanotubes(CNTs) by the decomposition of C_2H_2 over a thin catalyst film on an aluminium substrate. The precursor concentration, the time of deposition, the temperature and the ratio of C_2H_2:N_2 were greatly influenced in the density (mg cm^{-2}) and the length of the CNTs. The iron nitrate film formed an amorphous iron oxide layer that transformed to crystalline Fe_2O_3, which was reduced to Fe_3O_4 and FeO in contact with the C_2H_2:N_2 reaction atmosphere and the CNTs synthesis took place on small iron carbide (Fe_3C) particles that were formed from the FeO. The tip of the CNTs can be observed as iron carbide clusters [7].

M. C. Schnitzler et al. (2003) reported that using one-step route based on the pyrolysis of ferrocene or a ferrocene-$Fe_3(CO)_{12}$ mixture in a poor oxygen-containing atmosphere could provide produce iron and iron oxide-filled carbon nanotubes (CNTs), The reactor is using quartz tube with porous Vycor glass (PVG) as substrate. The results reveal the presence of CNTs, buckyonions and carbon nanopolyhedra, filled with α-Fe, Fe_2O_3 and Fe_3O_4. However, the higher iron oxide content on the samples growth on the PVG surface can be explained due to the presence of oxygen molecules previously entrapped inside the PVG pores. It is well known that the presence of metals like iron has an essential role in the formation of carbon nanotubes [8].

X. Wang et al. (2001) were successfully synthesized well-aligned carbon nanotubes by pyrolysis of iron (II) phthalocyanine using tube furnace reactor under argon and hydrogen atmosphere. They found that the outer diameter and the length of carbon nanotubes can be controlled by varying the growth time. The growth time varies from 2 to 60 min and the length of CNTs gradually increasing with the growth time. The grain size of iron catalyst plays an important role on the carbon nanotubes diameter since the catalyst grain size act as nucleation seed in the CNTs growth [9].

C.J. Lee et al. (2003) have produced well-aligned carbon nanotubes (CNTs) with high purity by pyrolysis of iron (II) phthalocyanine and acetylene at 800 ° C. The synthesized CNTs have a length of 75 μm and diameters ranging from 20 to 60 nm. The CNTs have a bamboo-like structure and exhibit good crystallinity of graphite sheets. The growth rate of the CNTs was rapidly increased with adding acetylene (C_2H_2). This method is suitable to large-scale synthesis of high-purity well-aligned CNTs on various substrates [10].

N. S. Kim et al. (2003) has found that CNTs were grown vertically aligned on silicon oxide substrates via the pyrolysis of FePc, CoPc, and NiPc in the temperature range 700-1000 °C. The average diameter of CNTs increases from 30 to 80 nm for the temperature increase from 700 to 1000 °C. Raman spectra reveals that the crystallinity of CNTs grown using NiPc is worse than that of the CNTs grown by using FePc and CoPc [11].

B.C. Satishkumar et al. (1999) have produced aligned nanotube bundles by the pyrolysis of ferrocene along with methane, acetylene or butane by using hydrocarbon gas as carbon source and ferrocene as catalyst precursor. From the results, ferrocene–acetylene mixtures are found to be ideal for the production of compact aligned nanotube bundles. The nanotube bundles are associated with iron nanoparticles of diameters in the range 2–13 nm. These nanoparticles are ferromagnetic, showing low saturation magnetization compared to bulk iron. The ferromagnetism of the transition metal nanoparticles is likely to be responsible for the alignment of the nanotubes [12].

D.C.Li et al. (2000) prepared the aligned carbon nanotubes by pyrolysis of iron II phthalocyanine (FePc) under Ar/H_2 atmosphere using a dual furnace fitted with independent temperature controllers. The pyrolysis temperature at 850°C for ca. 10 min is the best condition for preparing aligned carbon nanotubes. The TEM analysis indicates that the large iron particles are responsible for producing the carbon atomistic species required for the growth of the nanotubes and and the top of the carbon nanotubes is capped by iron particles [13].

2.3 Pyrolysis of organometallic compounds and additional carbon source

N. Sano et al. (2003) have shown that Fe-containing CNCs and CNTs were separately formed by pyrolysis of ferrocene in a pure hydrogen stream through a cylindrical furnace with a temperature profile controlled at 1050 °C in its center. The CNTs and CNCs were, respectively, formed at the zone with temperature of 988 °C and colder downstream zone of below 625 °C. The CNCs were observed to contain an iron carbide core. Typical CNC particle sizes were in the 11–30 nm diameter size range with 2–40 graphitic shells [14].

H.q. Hou et al. (2002) also reported that single-wall carbon nanotubes (SWCNTs) and well-aligned thin multi-walled carbon nanotubes (MWCNTs) were successfully synthesized via pyrolysis of a powder mixture of ferrocene and anthracene or 9, 10-dibromoanthracene. The size of the MWCNTs can be tuned just by changing the ratio of ferrocene/anthracene in the mixture. A lower ratio resulted in low-diameter MWCNTs containing up to only five graphene layers. However, a high ratio has led to thick MWCNTs with more than 25 layers and the pyrolysis of pure ferrocene in a hydrogen flow that mainly gives rise to metal nanoparticles. When powder mixtures of ferrocene and 9, 10-dibromoanthracene were pyrolyzed, both SWCNTs and spherical carbon-coated iron nanoparticles were obtained [15].

S. Bai et al. (2003) synthesized carbon nanostructures by a floating catalyst method. Carbon nanotubes (CNTs) and CNFs in different diameters and structures can be obtained by controlling the ferrocene (catalyst precursor)/benzene (carbon source) mole ratio and found that the diameter of CNFs and CNTs increases while mole ratio of ferrocene to benzene decreases. SWNTs can be synthesized when ferrocene/benzene mole ratio is around or above 15.1%. In the other way, MWNTs can be produced when ferrocene/benzene mole ratio is between 4.2% and 8.76% and CNFs can be synthesized when ferrocene/benzene is below 4.2% [16].

M.Endo et al. (2001) synthesized carbon nanofibers with diameters of 80–100 nm by the pyrolytic method when a benzene solution containing ferrocene was used as a feedstock. These fibers were manufactured by the decomposition of benzene using ferrocene as the catalyst. The sharp curvature caused by the small diameter prohibited perfect three dimensional graphene stacking during the graphitization process. Graphitization of the fibers was performed at 3000 ˚C for 30 min, using a graphite-resistance furnace operating in a high-purity argon atmosphere. Any amorphous carbon that was present was almost completely removed through an oxidization process [17].

S. Tomita et al. (2000) has reported the simple method for synthesizing graphitic carbon-coated magnetic-metal Co, Ni and Fe nanoparticles from annealing the mixture of metal and diamond nanoparticles at 1700°C in vacuum. TEM image shows that the thickness of the coating is uniform and around 3 nm. The spacing of the lattice fringes is about 0.34 nm, which is close to that of the graphite 002 planes. They found that the metal particles seem to play an important role for the transformation from diamond nanoparticles to the graphitic coating and graphitic coating starts at around 600 °C in the Co sample [18].

H. Zhang et al. (2003) has recently studied of reaction temperature and duration of the growth of aligned carbon nanotube arrays. Layered aligned multi-wall carbon nanotube (MWNT) films have grown directly by pyrolysis of ferrocene in xylene with the help of cobalt powder. The results indicated that the obtained products composed of many separated layers with MWNTs. The reaction temperature significantly influenced the alignment of the MWNTs, and an appropriate reaction temperature range for growth was 800–900°C. Besides temperature, the reaction duration influenced the length of the well-aligned carbon nanotubes [19].

Y. Lu et al. (2004) synthesized carbon-encapsulated Fe nanoparticles via a picric acid-detonation-induced pyrolysis of ferrocene. And they found the nanoparticles exhibit well-constructed core–shell structures, with bcc-Fe cores and graphitic shells and the graphitic shells can protect effectively the cores against the attack of HNO_3 solution. The core–shell nanoparticles are preferably formed at low C/Fe atomic ratios, while tubular structures are formed at high C/Fe ratio. Spheroidal Fe nanoparticles have a narrow diameter distribution of 5–20nm. From XRD analysis they could not found iron carbides in these products. The absence of carbides in these samples is possibly associated with the special high temperature environment [20].

H. Tokoro et al. (2004) have synthesized iron nanoparticles coated with graphite nanolayers by annealing mixtures of hematite and carbon under nitrogen atmosphere. Hematite is reduced to Fe_3O_4, FeO, and finally to iron completely at 1200 ˚C. The results reveal that the iron particles are coated with graphite nanolayers of 30 nm with 200 nm in diameter. It is noted that carbon nanotubes with diameter of 100 nm and length of a few micrometers are also synthesized during the process [21].

2.4 Mechanism of CNPs formation via pyrolysis

D.C. Li et al. (2000) have discussed on the growth mechanism which involved in two sizes of iron nanoparticles. While the small particle is catalytically active for the nucleation of the nanotube, the large particle produces the carbon atomistic species required for the growth of the nanotubes. From TEM analysis showed that the diameters of the nanotubes are significantly larger than those of the nanotubes grown at a lower temperature. The aligned nanotubes are believed to be the result of a competition growth process along the normal direction of the substrate. The surface diffusion of carbon atoms on the large iron particle leads to the formation of the observed bamboo-like structure [22].

Y. T. Lee et al. (2003) have grown aligned carbon nanotubes by pyrolysis of ferrocene and acetylene in the temperature range 700–1000^{o}C. As the temperature increases, the growth rate increases by 60 times and the relative amount of crystalline graphitic sheets increases significantly. However, the length of aligned CNTs reaches up to 3 mm at 1000^{o}C. The Arrhenius plot yields the activation energy 35±3 kcal/mol, which is close to the diffusion energy of carbon in bulk γ-Fe. It can be suggested that the bulk diffusion of carbons would play an important role in the growth of cylindrical structured carbon nanotubes [23].

A. Gorbunov et al. (2002) have suggested the mechanism of formation of the single wall carbon nanotubes by solid-liquid-solid model. The SWNTs growth mechanism is a kind of solid–liquid–solid graphitization of amorphous carbon or other imperfect carbon forms catalyzed by molten supersaturated carbon–metal nanoparticles. The melting of the catalytic nanoparticles leads to a pronounced increment of carbon solubility which alters the character of the interaction of the precipitated graphitic form of carbon with the catalyst surface, and presumably can result in a SWNTs nucleation [24].

X.X. Zhang et al. (2001) have studied on the magnetic properties of iron nanoparticles partially encapsulated at the tips of aligned carbon nanotubes which prepared by pyrolysis of FePc under argon and hydrogen atmosphere. The carbon nanotube wall not only protects the metallic particles from oxidization, but also reduces the inter-particle dipolar interaction by non-magnetic separation. The magnetic characterizations performed in the temperature range of 5–350K with magnetic field up to 3 T shown that these carbon-nanotube-supported iron particles are good candidates for high-density magnetic recording media [25].

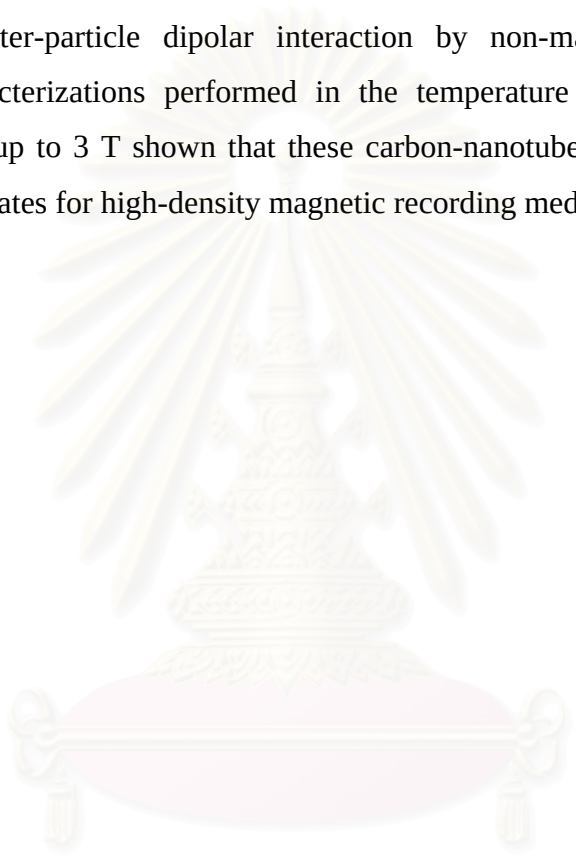

CHAPTER III

THEORY

3.1 Carbon nanoparticles (CNPs)

Since the first discovery of $C_{60,}$ Buckminsterfullerene, by H. Kroto and R. Smalley in 1985, it has initiated substantial attentions in many research areas particularly those of synthesizing carbon nanoparticles (CNPs) such as nanotubes (CNTs), nanohorns (CNHs), nanocapsules (CNCs) and so on. Among these structures, carbon nanotubes (CNTs) are currently the subject of intense research because of their extraordinary mechanical and electrical properties.

3.1.1 Buckminsterfullerene (C_{60})

The 60 carbon atoms in C60 are located at the vertices of a regular truncated icosahedron, 0.710 nm in diameter. Every carbon site on the C60 molecule is equivalent to every other site (see Fig. 3.1). The average nearest neighbor carbon-carbon (C-C) distance in C60 is very small (0.144 nm) and is almost identical to that in graphite (0.142 nm). Each carbon atom in C60 (and also in graphite) is trigonally bonded to three other carbon atoms, and 20 of the 32 faces on the regular truncated icosahedron are hexagons, the remaining 12 being pentagons. Thus we may consider the C60 molecule as a "rolled-up" graphene sheet (a single layer of crystalline graphite) which forms a closed shell molecular nanostructure, in keeping with Euler's theorem, which states that a closed surface consisting of hexagons and pentagons has exactly 12 pentagons and an arbitrary number of hexagons. The introduction of pentagons gives rise to curvature in forming a closed surface. To minimize local curvature, the pentagons become separated from each other in the self-assembly process, giving rise to the isolated pentagon rule, an important rule for stabilizing fullerene clusters.

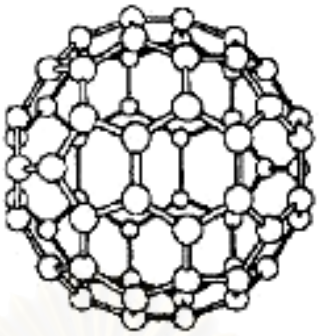

Figure 3.1 $C_{60,}$ Buckminsterfullerene [26]

3.1.2 Carbon nanotubes (CNTs)

Carbon nanotubes can be considered as elongated fullerene. It could be noted that there are 6 pentagons in each end of tube so that a hexagonal graphene sheet is able to close as shown in Figure 3.2(right). Two types of CNTs can be categorized if considering the types of CNTs wall. One is single-walled carbon nanotubes (SWCNTs). Another is multi-walled carbon nanotubes (MWCNTs). Interestingly, these nested tubes exhibited interlayer spacings of 3.4 A°, a value that is slightly greater than that of graphite (3.35 A°). Iijima attributed this difference to a combination of the tubule curvature and van der Waals interactions between the successive cylinders. It is also important to note that, probably, the first images of carbon nanotubes were obtained by M. Endo and co-workers in the mid-1970s. In their paper, it was reported that by pyrolysis of benzene and ferrocene at 1000˚C, it was possible to obtain tubular graphite of nanometre scale.

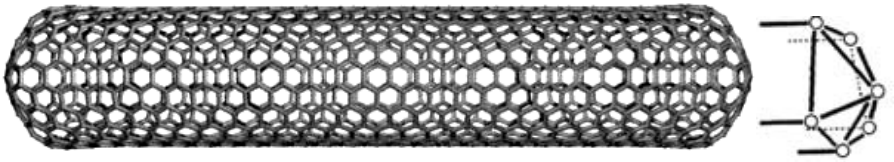

Figure 3.2 Model of single-walled Carbon nanotube (SWNT) (left), nanotube tip exhibiting regions where 6 pentagonal rings are located (right) [26]

3.1.2.1 Structure of carbon nanotubes

Theoretically, it is possible to construct a carbon tube by rolling up a hexagonal graphene sheet in various ways. Two of these are ‘non-chiral’, so that the honeycomb lattices located at the top and bottom of the tube are always parallel. These configurations are known as ‘armchair’ and ‘zigzag’. In the armchair structure, two C–C bonds on opposite sides of each hexagon are perpendicular to the tube axis, whereas, in the zigzag arrangement, these bonds are parallel to the tube axis (Fig. 3.3, b). All other conformations, where the C–C bonds lie at an angle to the tube axis, are known as ‘chiral’ or helical structures (Fig. 3.3 c).

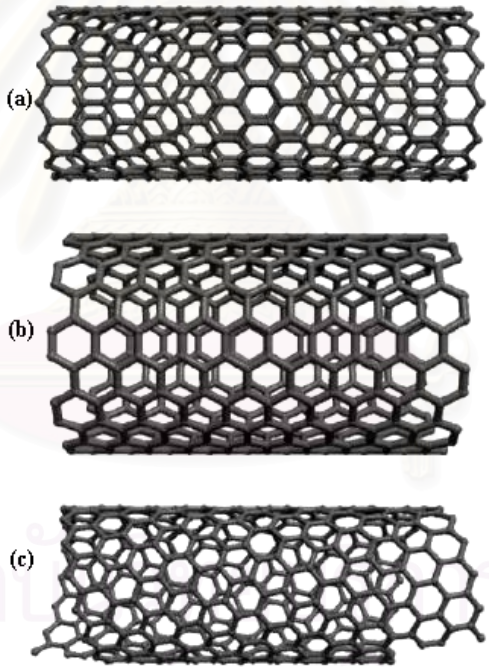

Figure 3.3 Molecular models of SWNTs exhibiting different chiralities
a) zigzag arrangement; b) armchair configuration; c) chiral conformation [26]

At present, carbon nanotubes can be obtained using various techniques: arc discharge, pyrolysis of hydrocarbons over catalysts, laser and solar vaporisation, and electrolysis. These nanoscale materials can exhibit different morphologies such as straight, curled, hemitoroidal, branched, spiral, helix-shaped, etc. In 1992, two groups

predicted theoretically that single-walled carbon nanotubes (SWNTs) might be metallic or semiconducting carbon nanowires, depending upon their helicity and diameter (Hamada and Saito et.al).

Recent examples of applications (see Figure 3.4) include the use of carbon nanotubes as:

- gas storage components of argon, nitrogen, and hydrogen
- AFM probes (Figure 3.4 d) and field emission sources(Figure 3.4 c)
- high power electrochemical capacitors
- electronic nanoswitches
- chemical sensors
- magnetic data storage (e.g. iron filled nanotubes)
- nanocomposites (Figure 3.4 a), etc.

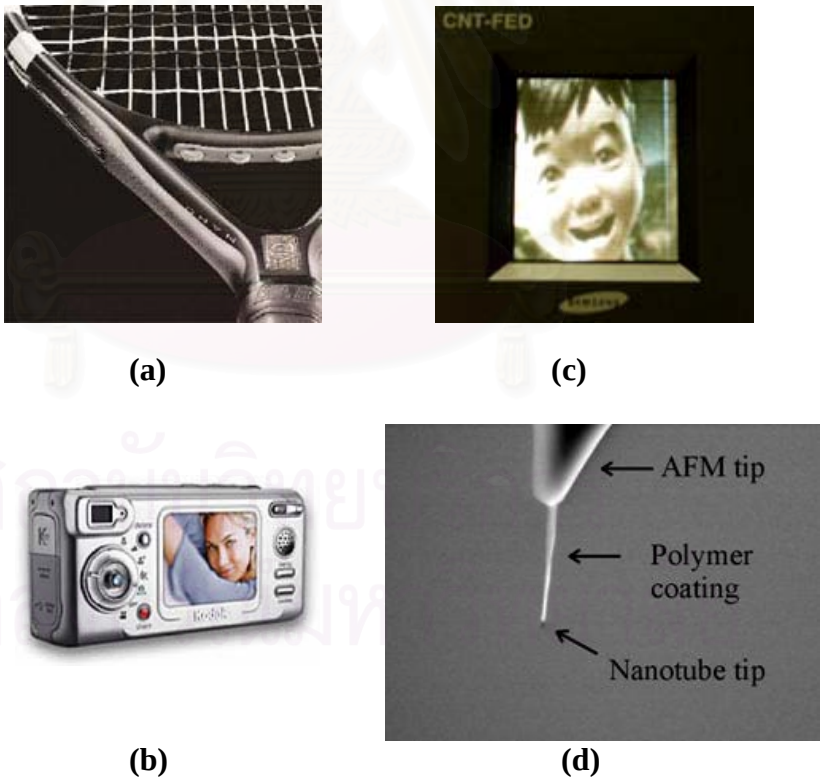

Figure 3.4 Applications of carbon nanotubes: a) Tennis Racquet; b) Digital camera (Easy Share LS633); c) CNT-FED television; d) AFM tip

3.1.3 Carbon Nanocapsules (CNCs)

It has been suggested that carbon-coated magnetic nanoparticles might have important applications in areas such as magnetic data storage, xerography and magnetic resonance imaging. A typical example of carbon nanocapsule is shown in Fig. 3.5. It is a particle containing Fe encapsulated by graphene layers. The role of the carbon layer would be to isolate the particles magnetically from each other, thus avoiding the problems caused by interactions between closely spaced magnetic bits, and to provide oxidation resistance. In addition, the lubricating properties of the graphitic coatings might be helpful in magnetic recording and applications. The potential of important applications has motivated a significant amount of research on the encapsulation of magnetic materials in carbon nanoparticles.

Carbon nanocapsules which there are no metal as core particle can be called as multi-shelled nanoparticles. These particles consist several of graphene sheets in various shapes such as spherical, polyhedral, or short-tube.

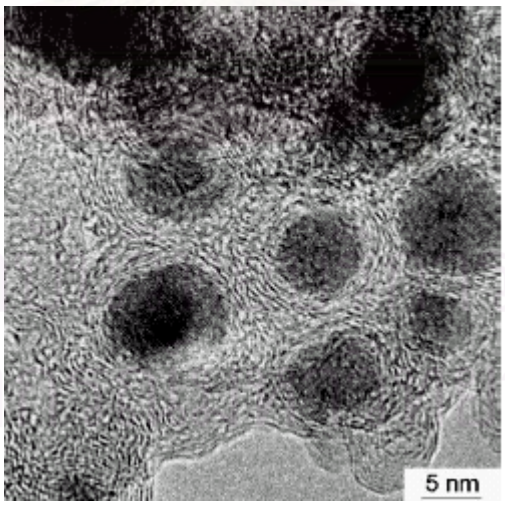

Figure 3.5 Carbon nanocapsules with iron particles in core [20]

3.1.4 Carbon nanohorn (CNHs)

Another type of carbon nanoparticles is named nanohorns due to their irregular horn-like shape, and were discovered by Sumio Iijima's research group. Nanohorns have the same graphitic carbon atom structure as normal carbon nanotubes. The main characteristic of the carbon nanohorns is that when many of the nanohorns group together an aggregate (a secondary particle) of about 100 nanometers is created. The advantage being, that when used as an electrode for a fuel cell, not only is the surface area extremely large, but also, it is easy for the gas and liquid to permeate to the inside. In addition, compared with normal nanotubes, because the nanohorns are easily prepared with high purity it is expected to become a low-cost raw material.

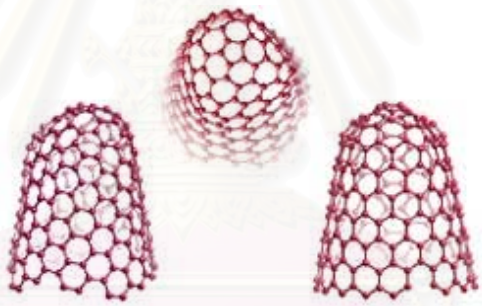

Figure 3.6 Carbon nanohorns (CNHs) model

3.2 Production Methods

As mentioned above, carbon nanotubes (single or multiwalled) and other nanoparticles can be produced using different methods. Each technique offers advantages and disadvantages. It can be accepted that pyrolysis of organometallic compounds as ferrocene has been well proved to be a promising way towards not only multi-wall nanotubes, single-wall nanotubes, but also carbon-encapsulated iron nanoparticles. However, it is worth mentioning that CVD or thermal pyrolysis play an important role in the mass production of carbon nanotubes. The methodology has summarized as follow.

3.2.1 Hydrocarbon Pyrolysis

Pyrolysis is formally defined as chemical decomposition induced in organic materials by heat in the absence of oxygen. Thermolysis or pyrolysis of hydrocarbons (e.g. methane, benzene, acetylene, naphthalene, ethylene, etc.) in the presence of metal catalysts (e.g. Co, Ni, Fe, Pt, and Pd deposited on substrates such as silicon, graphite, or silica) offers an alternative route to fullerenes, carbon nanotubes and other fascinating nanostructures. As mentioned above, pyrolytically grown carbon nanofibres/nanotubes have actually been observed and structurally identified by several authors. The hydrocarbon pyrolysis process is also known as chemical vapour deposition (CVD).

3.2.1.1 Growth of aligned carbon nanotubes

Ajayan and co-workers [26] were the first to align MWNTs by cutting thin slices (50–200 nm thick) of a polymer/nanotube composite. The aligning effect was caused by the mechanical deformation suffered, during cutting, by the MWNTs embedded in the polymer. Unfortunately, this type of nanotube alignment depends on the thickness of the polymer slice, and the process becomes impractical for aligning large areas of carbon nanotubes. Subsequently, De Heer and colleagues [26] managed to align MWNTs (produced using arc techniques) by rubbing the nanotube powder on a substrate. However, other methods to grow and align nanotubes in large areas using self-assembly processes could also be used (see below).

3.2.1.1.1 Aligned nanotubes on patterned substrates

By the end of 1996, Li et al. [26] had described the large scale synthesis of aligned MWNTs, of uniform length and diameter by passage of acetylene over iron nanoparticles embedded in mesoporous silica at elevated temperatures. Furthermore, Ren and co-workers subsequently demonstrated that aligned MWNTs could also be generated using plasma enhanced chemical vapour deposition techniques: by

thermolising acetylene over iron nanoparticles embedded in mesoporous silica, at temperatures above 700˚C. It is noteworthy that all the above methods, based on the pyrolysis of organic precursors over templated/catalyst supports, are by far superior when compared to carbon arc discharge techniques, because graphitic polyhedral particles, encapsulated metal particles and amorphous carbon are notably absent.
Consequently, numerous groups started to develop alternative routes to aligned MWNTs based on pyrolytic methods. In this context, microwave plasma enhanced chemical vapour deposition has now been widely used to grow continuous carpets of aligned carbon MWNTs using different substrates (Si, SiOx, etc.), carbon sources (methane, acetylene, ethylene, CO2, etc.), and metal catalysts (Ni, Co, Fe) at different temperatures (450– 750˚C).

3.2.1.1.2 Aligned nanotubes in absence of patterned substrates: self-assembly techniques

a) Pyrolysis of solid organometallic precursors

Rao and co-workers [26] demonstrated that aligned MWNTs could be grown by the simple thermolysis of ferrocene powder using a two-stage furnace system. This process was carried out in the absence of patterned catalytic substrates. Soon after, many researchers have developed a continuous production process for generating MWNT arrays by thermolysing ferrocene–hydrocarbon solutions at different temperature.

Pyrolysis of solid carbon-containing precursors, together with ferrocene (or mixtures with other metallocenes), also yields aligned nanotubes with iron (or metal alloys) encapsulated in the cores of graphene cylinders. However, C60 can also be used as a source of pure carbon in the ferrocene experiments. In this case, highly crystalline aligned carbon nanotubes are produced. Similar reports have been published regarding the production of aligned MWNTs using the thermolysis of solid precursors involving ferrocene together with other carbon containing compounds. It is important to note that the pyrolysis of nickelocene or cobaltocene has never been proved successful in the production of aligned nanotube bundles. It is important to

mention that some of these organometallic compounds are highly toxic, and special measures should be taken when carrying out such experiments.

b) Pyrolysis of solutions of organometallic precursors

Thermolytic processes of sprayed solutions containing ferrocene and organic solvents have proved extremely efficient in producing bulk amounts of aligned MWNTs. Argon is also employed to regulate the liquid flow directed to the nozzle during spraying. The benzene–ferrocene solution (Kamalakaran et al) was subsequently ‘atomised’, forming a spray, by flowing argon around the nozzle (Fig.3.7).

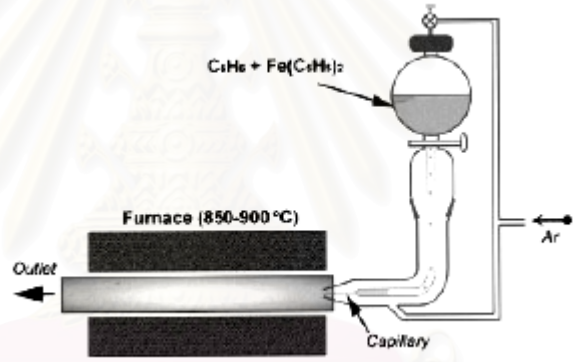

Figure.3.7 Schematic of pyrolysis ferrocene-benzene set-up for synthesis of aligned MWNTs [26]

3.2.1.2 Mechanism of carbon nanoparticles formation

Various researchers have proposed mechanisms to account for carbon nanotube growth by pyrolysing hydrocarbons over metal catalysts. The following mechanisms are now widely recognised.

1. Top carbon diffusion ‘through’ catalytic particles which Baker and co-workers postulated that decomposition of acetylene on the exposed surfaces of the metal catalyst resulted in the formation of bimolecular hydrogen and carbon species.

The carbon then diffuses through the catalytic particle and precipitates at the other end of the filament (Fig. 3.8 a). The exothermic nature of hydrocarbon decomposition results in a temperature gradient across the catalyst, which appears to be a crucial factor associated with the model in question. Thus, carbon is precipitated at the colder zone of the particle, allowing the filament to grow (Fig. 3.8, b, c). This process continues until the catalytic activity of the leading particle is neutralised (Fig. 3.8 d).

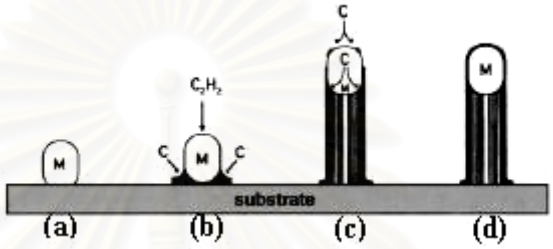

Figure 3.8 Growth mechanism for formation of C nanotubes by pyrolysis of acetylene (C_2H_2) on metal particle (M) (Baker and Harris) [26]

2. Top carbon diffusion ‘on’ catalytic particles (Baird and Fryer in 1974 and Oberlin et al. in 1976) proposed that carbon filaments are formed by surface diffusion on the particle (Fig. 3.9). The figure illustrate growth mechanism proposed for C fibres and filaments from benzene pyrolysis over catalytic particles hydrocarbon is cracked on surface of metal and diffuses on surface of particle, C then precipitates at colder end in form of graphitic domains.

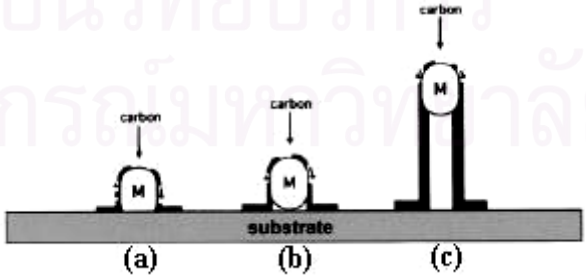

Figure 3.9 Growth mechanism from benzene pyrolysis over catalytic particles (Oberlin et al.) [26]

3. Bottom carbon diffusion ‘through’ catalytic particles. This mechanism was based upon pyrolytic decomposition of acetylene passed over Fe–Pt substrates and by natural gas passed over stainless steel surfaces at high temperatures. In the latter case, growth occurs due to the rapid movement of carbon through the catalyst by a diffusion process, thus generating a filament (Fig. 3.10). In this model, tubes grow from their bases rather than from their tips which C also diffuses through metal, but particle always remains at bottom of filament

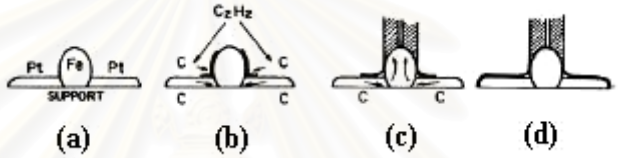

Figure 3.10 Growth Mechanism for Carbon nanotube growth from Fe–Pt/C_2H_2 systems (Baker and Harris) [26]

However, it is worth mentioning that CVD plays an important role in the mass production of carbon nanotubes. Most commercially available carbon nanotubes are synthesised using this type of route. For example, Hyperion Catalysis International, Inc. (Cambridge, MA) started the large scale production of MWNTs in the 1990s. HiPCo SWNTs, developed by Smalley and co-workers at Rice University, can also be purchased commercially. Carbon Nanotech Research Institute (CNRI), a subsidiary of Mitsui & Co.,Ltd, plans to engage in developing technologies for the large scale production of 120 t of MWNTs annually. Others companies, such as Applied Sciences, Inc. (API) and Showa Denko (SDK), already have a large scale production capacity for MWNTs, which exhibit relatively large diameters and a wide distribution of diameters in the range 70–200 nm.

CHAPTER IV

EXPERIMENTAL

4.1 Experimental setup

The preliminary part of this work is constructing an experimental apparatus for synthesize of carbon nanoparticles. Although, there are many investigations which use tube furnace with dual and single furnace reactor for pyrolysis of various carbon source. But both of them have the difference in controlling of temperature profile of the tube. For dual furnace reactor, the first furnace is used for controlling the vaporization temperature of the raw materials used and the other is used for controlling the pyrolysis temperature. The disadvantage of dual furnace is the uncontinuity of temperature profile in the tube which having more effect on the structure of CNPs. However, the single furnace can provide the continuity of temperature profile in the tube than dual furnace reactor although it has a problem in controlling the vaporization temperature of the raw materials used.

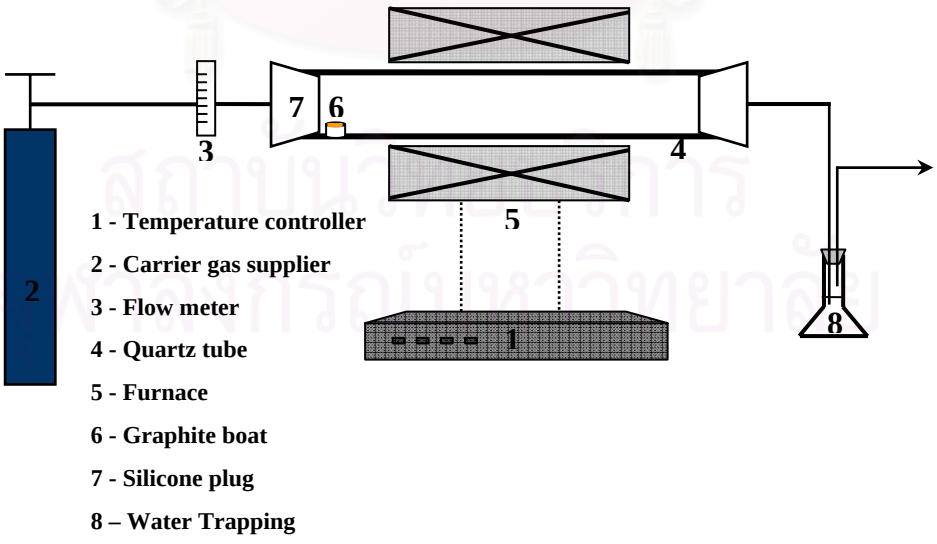

Figure 4.1 Experimental apparatus for thermal co-pyrolysis of ferrocene and naphthalene mixture

For this work, A single furnace reactor is applied from Sano's work [2]. The experimental apparatus has shown in Figure 4.1. It is consisted of tube furnace reactor (Figure 4.2) equipped with temperature controller (Figure 4.3) for controlling the pyrolysis temperature between 800 ˚C to 1050 ˚C. Quartz glass tube with 4.5 cm outer diameter and 65 cm length (Figure 4.4) has used for co-pyrolyzing the mixture of raw materials. The gas supplier will provide carrier gas during the pyrolysis process and silicone plug (Figure 4.5) has been used for preventing the process from other gas. The gas from the process will be removed by trapping with water before purging to outside.

Figure 4.2 Tube furnace reactor

Figure 4.3 Temperature controller

Figure 4.4 Quartz glass tube

Figure 4.5 Silicone Plug

4.2 Experimental Procedure

Tube furnace apparatus shown in figure 4.1.1 is employed for co-pyrolyzing mixture of ferrocene and naphthalene to synthesize carbon nanoparticles. The apparatus consists of a single-stage furnace equipped with temperature controller and quartz glass tube (inner diameter, 41 mm). The carrier gas (nitrogen 99.99% or argon 99.995%) is fed continuously through a flow meter at desired flow rate. The experimental procedures are shown as follows,

a) The furnace will be set the temperature at desired condition by using temperature controller.

b) Ferrocene (Sigma-Aldrich, ≥98% Fe) 280 mg and naphthalene (Ajax Chemicals) at various quantities are mixed to adjust a specific molar ratio (1:1, 1:2 and 1:5 of ferrocene to naphthalene) and then are loaded into a graphite boat which is placed at the entrance of the quartz tube where the temperature is kept above the vaporization temperature of the mixture (100˚C).

c) The decomposition of the mixture occurred at about 400˚C and free carbon and iron vapor are carried over by the carrier gas at desired flow rate through the tube into the hot zone where self-assembling and catalytic growth reactions took place.

d) Large quantities of the as-grown deposit films as in Figure 4.6 can be found as accumulation along the inner surface of the quartz tube after reaction complete (30 min). The detailed experimental parameters are presented in Table 4.2.

Table 4.1 The parameters for co-pyrolysis work studied

F[a]:N[b] molar ratio	**Amount of F/N (g)**	**Carrier gas**	**Temperature range (˚C)**
1:1	0.2804/0.1937	N_2 and Ar	800 - 1050
1:2	0.2804/0.3864	N_2 and Ar	800 - 1050
1:5	0.2804/0.9659	N_2 and Ar	800 - 1050

[a]Ferrocene, [b]Naphthalene

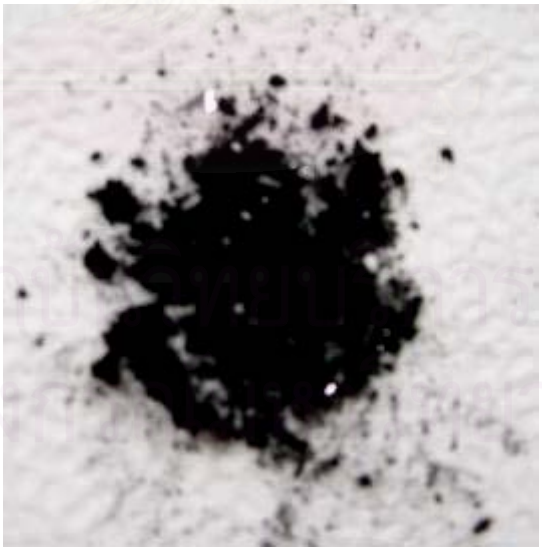

Figure 4.6 As-grown carbon nanoparticles obtained from co-pyrolysis process

4.3 Analytical Instruments

The morphology of the as-grown samples was first analyzed by Field Emission Scanning electron microscope (FESEM; HITASHI S-900). The structure and crystallinity of the as-grown samples were investigated by Transmission Electron Microscope (TEM; JEOL2010). The overall crystallinity of CNPs was evaluated by Raman analysis (Renishaw Ramascope System 2000).While dynamic light scattering (DLS; MALVERN, ZETASIZER 300HSA) is employed for determining particles size distribution of the obtained products.

4.3.1 Field Emission Electron Microscopy (FESEM)

The microstructure of the carbon nanoparticles were studied by using Scanning Electron Microscopy (SEM), Hitachi S-900 (Figure 4.7) equipped with a field emission source. The specimen used for SEM analysis was either from the as-grown film or scratched (Figure 4.6). The sample was prepared by grinding using a granite mortar and then the appropriate amounts of the prepared sample were mounted on carbon tape. The specimens were loaded into the sample chamber and then the observation was conducted immediately with using image catcher scanner for taking the photos.

Figure 4.7 Field Emission Scanning Electron Microscope (FESEM)

4.3.2 Transmission Electron Microscopy (TEM)

TEM analysis used in this work is JEOL-2010 as shown in Figure 4.8. The specimen for analyzing was elaborately prepared by grinding as-grown solid deposit (Figure 4.6) by a granite mortar. The appropriate amounts of carbon nanoparticles were suspended in toluene before ultrasonic treatment with the sufficient time (15 min) for ensuring its uniform dispersion. A few drop of clear solution was poured onto a microgrid covered with a carbon thin film (Figure 4.9). The specimen was loaded into sample chamber and waiting for the vaccum condition and steady state inside the chamber for 30 min.

Figure 4.8 Transmission Electron Microscopy (TEM)

Figure 4.9 Copper grid coated with carbon films for Transmission Electron Microscopy

4.3.3 Dynamic Light Scattering (DLS)

For particle size distribution analysis, Dynamic Light Scattering (DLS) using ZETASIZER 300HSA as shown in Figure 4.10 was employed. It should be noted that DLS is based on the measurement of the dispersion of light scattering by particles motion in a static solvent such as toluene, water, acetone or ethanol, the measured particle size should correspond to hydrodynamic diameter but not to the real diameters of the particles with complex structures. However, DLS results were expected to give at least the qualitative trend in particle sizes distribution. For preparation of the sample, DLS specimens were also prepared by grinding as-grown particles (Figure 4.6) by the granite mortar and then suspended in toluene before ultrasonic treatment with the sufficient time (15 min) for ensuring its uniform dispersion. Afterwards, the specimen was diluted by toluene again until they became transparent and ultrasonicated again for 15 min before loading to the sample cell for analysis.

Figure 4.10 Dynamic Light Scattering (DLS)

4.3.4 Raman Spectroscopy

As-grown substrate of solid deposit was filled into the hole of specimen holder and then was bombarded by an Ar ion laser (514.5 nm) at the room temperature. In the cases of carbon nanoparticles (CNPs), two peaks can be found in the wavenumber between 1200 and 1800 cm^{-1}. One is a strong peak at 1590 cm^{-1} (Graphite band, G band) arises from an in-plane oscillation of carbon atoms in the sp^2 graphene sheet. Another is a weak peak at 1340 cm^{-1} (Disordered band, D band) reflects the degree of defects or dangling bonds contained in the sp^2 arrangement of graphene sheet. The Raman spectroscopy machine is shown in Figure. 4.11.

Figure 4.11 Raman Microscope (Renishaw Ramascope System 2000)

CHAPTER V

RESULTS AND DISCUSSION

5.1 Effect of pyrolysis temperature

5.1.1 Temperature profile of the tube

Since a tube reactor is employed in this study for pyrolysis of ferrocene and naphthalene mixture the temperature profile along the axial direction of the reactor is a crucial parameter to be known before conducting other experiments. The temperature profile can be determined by using thermocouple (type K) as shown in Figure 5.1 meanwhile the same type of thermocouple with different length has been used for controlling pyrolysis temperature at the middle of the tube. In practice, both thermocouples were calibrated to confirm their response. The calibration curve is shown in Figure 5.2. The temperature profile has been determined by inserting the thermocouple into the tube and shifted its tip for 1 centimeter after achieving the steady state condition. The temperature profile for each temperature sitting in this work (800°C to 1050°C) has been shown in Figure 5.3. Each curve exhibits a symmetric distribution and a maximum value is at the middle of the tube. Because the temperature profile changes with respect to each condition, correspondingly the position of raw material container has been changed. In practice, the mixture of ferrocene and naphthalene contained in a graphite boat was placed at the position of which temperature is 150°C in every experiment because it is the condition that the mixture could be vaporized without decomposition.

Pyrolysis process has been started by vaporization of the mixture and carrier gas will carry the vapors to the downstream zone where the decomposition could take place. After the growth time of 30 minutes, the obtained product is collected by peeling from the tube wall. The products have been characterized by electron microscopy, DLS, Raman spectroscopy and XRD.

Figure 5.1 Thermocouple type K

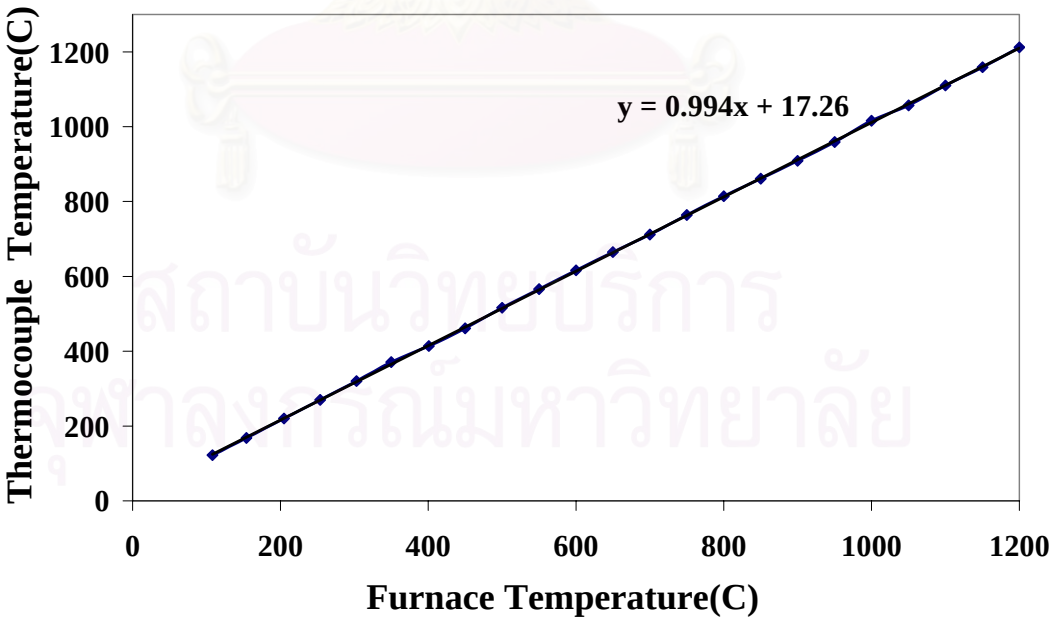

Figure 5.2 Calibration curve of thermocouple

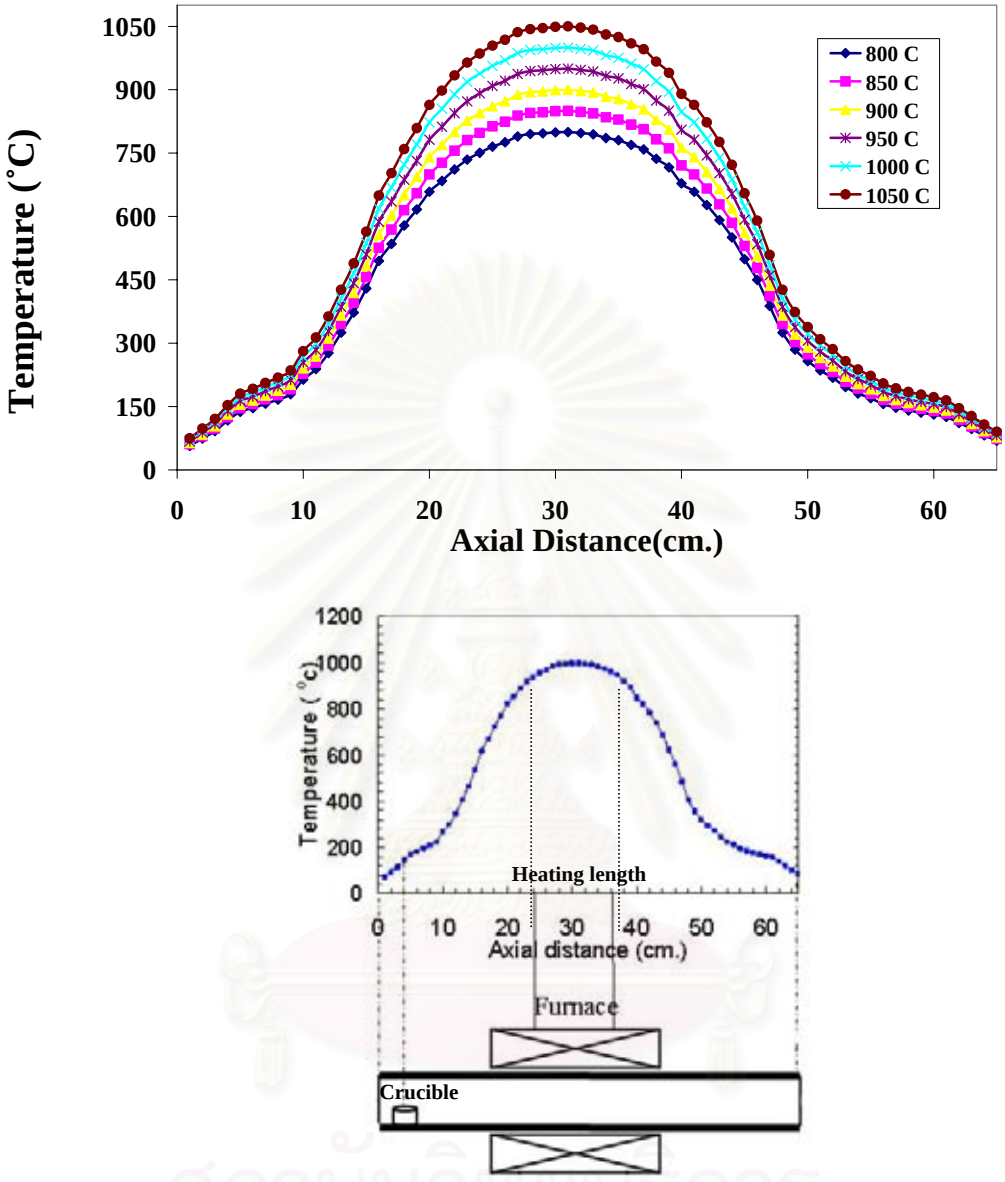

Figure 5.3 Temperature profile for each pyrolysis temperature

5.1.2 Microscopic analysis

5.1.2.1 SEM and TEM analysis

As the result from co-pyrolysis process, a layer of dark film fully covers the surface of quartz tube. The dark film was scraped from the quartz surface for SEM and TEM analysis.

From SEM observation, the as-grown black film consists of large amount of entangling carbon nanotubes (CNTs) as shown in Figure 5.4. Under a condition of pyrolysis at 800 °C and a total growth time of 30 min, the obtained product is CNTs with diameters of 40 to 80 nm with length of several ten microns. However, with the pyrolysis temperature of 850°C at the same molar ratio of ferrocene and naphthalene, densely packed carbon nanotubes aligned perpendicular to the substrate could be obtained as shown in Figure 5.5. The carbon nanotube array exhibits a uniform thickness and tube length. The tubes are straight and well-aligned with the length of 50 μm. However, some agglomerations of very fine particles also deposit on the tube tube bundle surface. On the top edge of the tube bundles, there are many fine particles with different morphology. It would be able to verify later that those particles are iron clusters encapsulated in carbon shell.

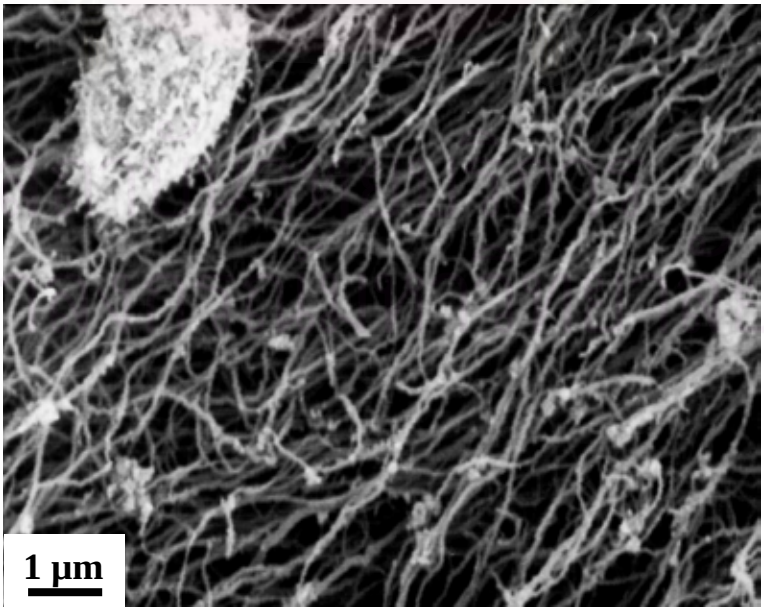

Figure 5.4 SEM image of CNTs at 800°C and 1:1 molar ratio of mixture

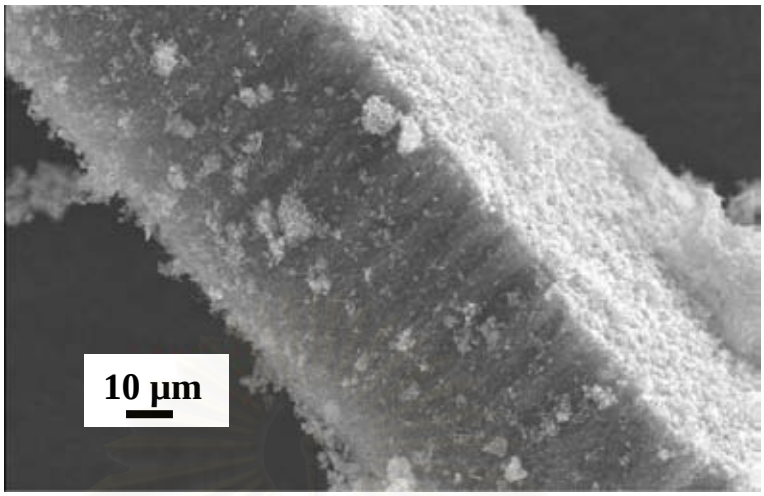

Figure 5.5 SEM image of CNTs at 850°C and 1:1 molar ratio of mixture

When the pyrolysis temperature is rose up to 1000 and 1050 °C as could be seen in Figures 5.6 and 5.7 the obtained products are composed mainly of spherical carbon nanocapsules mixed with carbon nanotubes. At 1000°C (Figure 5.6) most of the obtained products are spherical carbon nanoparticles with few carbon nanotubes. The obtained CNTs are not straight and well-aligned as formed in the conditions of lower temperature. The tube diameter is between 20 to 80 nm with length of 2-3 microns while the spherical particles have a broad distribution of diameters ranged from 80 nm to 400 nm. From Figure 5.7, at the highest temperature of 1050°C most of the obtained products are carbon nanoparticles with larger diameters of more than 100 nm.

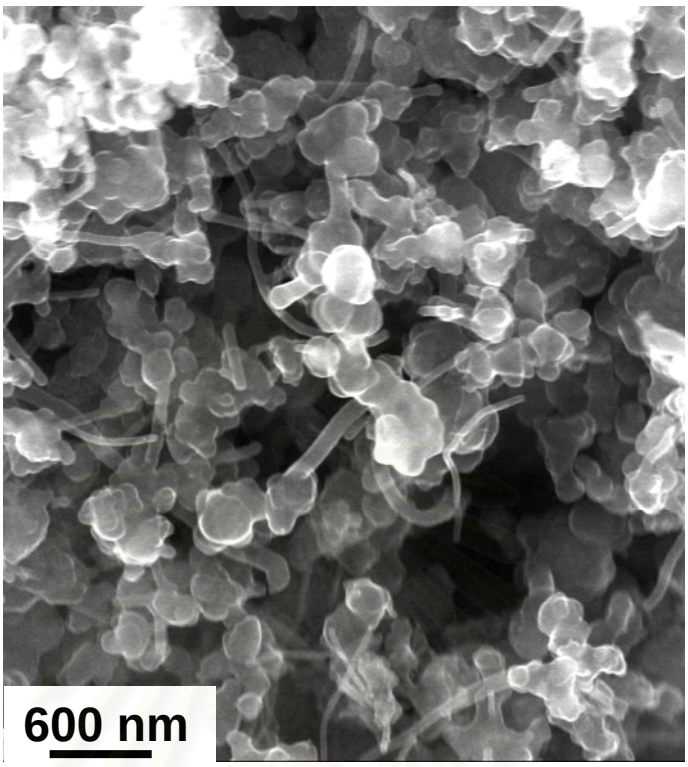

Figure 5.6 SEM image of CNTs at 1000°C with molar ratio of 1:1

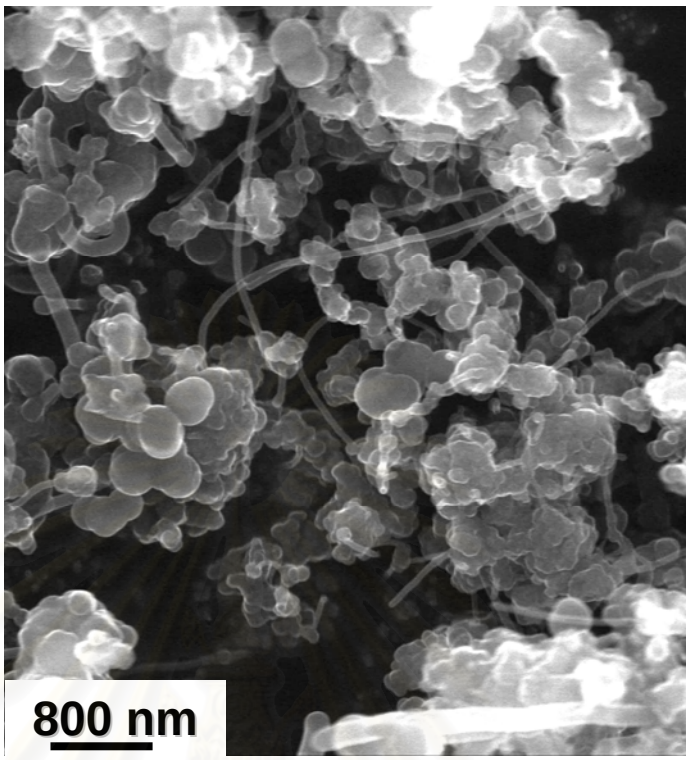

Figure 5.7 SEM image of CNTs at 1050°C with molar ratio of 1:1

For further investigation of the microstructure of the synthesized products, a carefully sampled product is dispersed in toluene and ultrasonicated before dropped on a copper grid for TEM observation. As shown in Figure 5.8, the low magnification of the TEM image of the product obtained at 800 °C illustrates that most of the obtained particles are CNTs with diameters of 20-40 nm. Moreover, the obtained CNTs are multiwalled carbon nanotubes (MWCNTs) with iron particles filled in the tubes and at the tube tip. It is in good agreement with the SEM observation that the as-grown black film consists of large amount of entangling carbon nanotubes.

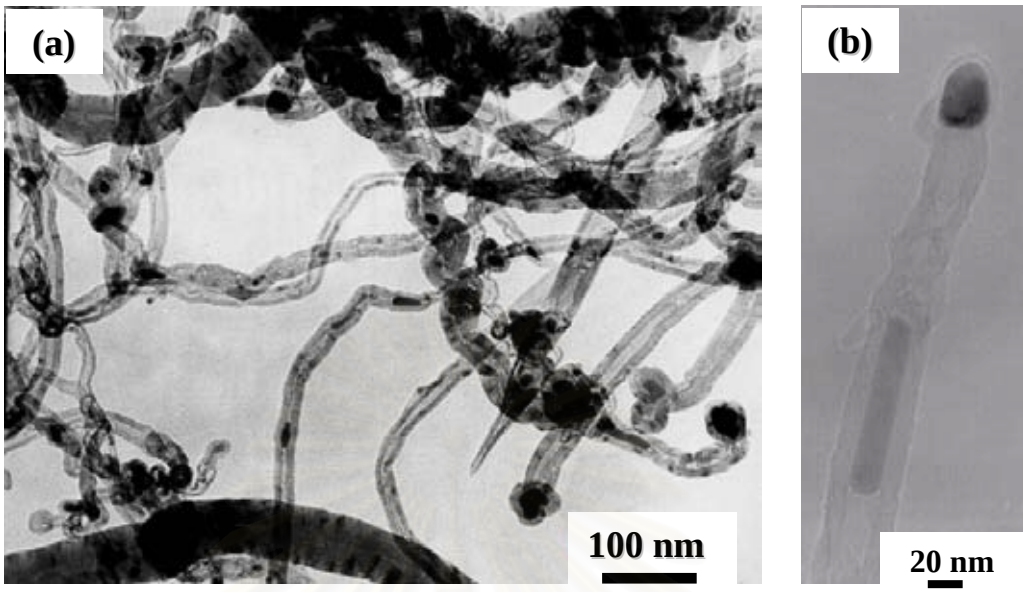

Figure 5.8 (a) TEM image of CNTs at 800°C with molar ratio of 1:1. (b) CNTs with iron particle in the tip

Higher magnification of TEM images of CNTs obtained at 850 °C also reveals that the obtained nanotubes are multi-walled carbon nanotubes (MWCNTs) with 16 layers of graphene sheets as shown in Figure 5.9 (b). The obtained MWCNT has graphite structure with the interlayer spacing of about 0.35 nm which is close to that of the graphite (002) planes. The obtained nanotube consists of axially symmetrical graphite shells. Under other observations, the number of graphite shells varies from 12 to 21 layers. Each nanotube has iron particles wrapped inside as shown in Figure 5.8 (b). It suggests that these products are obtained from the growth of carbon atoms induced by iron clusters.

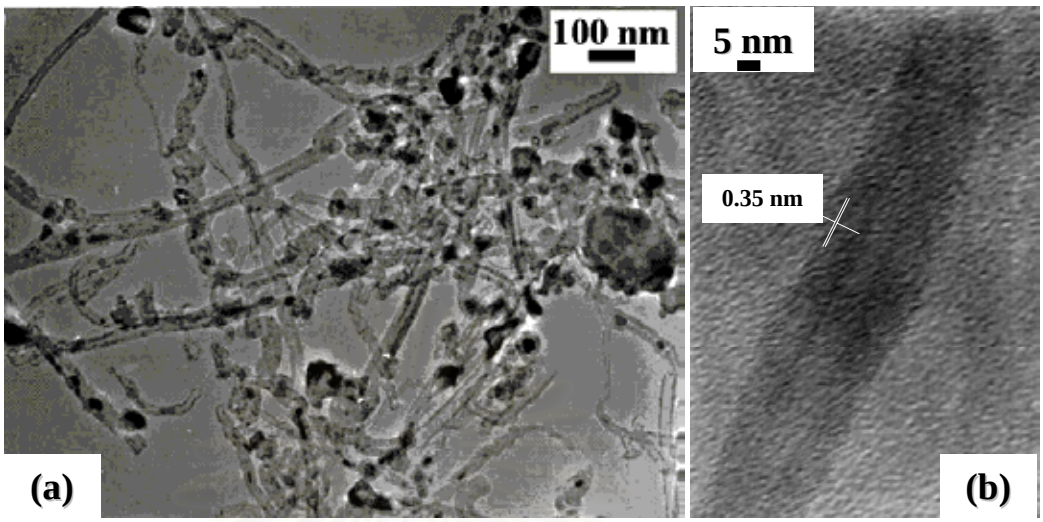

Figure 5.9 TEM image of CNTs at 850°C and 1:1 molar ratio of mixture. The low magnification TEM image indicated MWCNTs with iron particles (left). The high magnification image of CNTs showing good crystallinity of graphite sheets (right).

Interestingly, from TEM observation of the as-grown products obtained from higher temperature, most of products are nanoparticles with iron wrapped within the graphitic shells as shown in Figure 5.10. The CNCs have diameters ranged between 10 to 30 nm with iron particles encapsulated inside. At higher temperature, diameter of CNCs increases due to coalescence of the active catalytic particles as shown in Figure 5.10 (b).

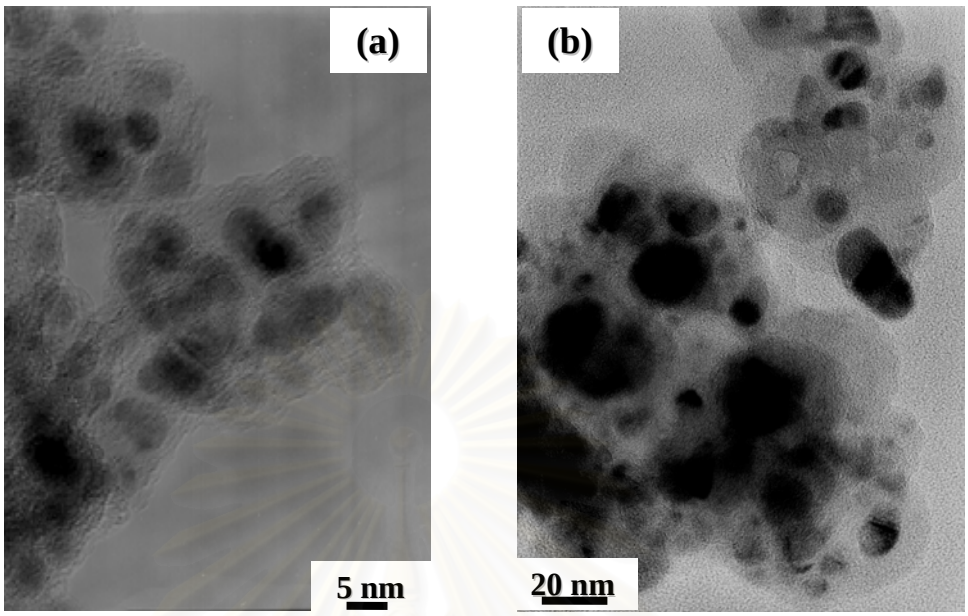

Figure 5.10 TEM image of CNCs at 1000°C, 1050°C and 1:1 molar ratio of mixture. (a) TEM image indicated CNCs with iron particles (left). (b) TEM image of CNCs with larger particles diameter (right).

5.1.2.2 Elemental analysis

5.1.2.2.1 The energy dispersive X-ray (EDX)

The energy dispersive X-ray (EDX) spectroscopic analysis has been performed for elemental analysis as shown in Figure 5.11. It is found that the top ends of the CNTs were composed mainly of carbon and Fe. This indicates that the obtained CNTs are generated by the so-called tip growth mechanism. With this mechanism, the metallic iron particles are lifted up as carbon atoms come to the reaction site, resulting in the CNTs growth. The EDX spectrum also reveals that the CNCs obtained from pyrolysis of ferrocene-naphthalene mixture are similarly composed of carbon and Fe as shown in Figure 5.12. However, because of the increasing fraction of carbon atoms, intensity of peak indicating presence of Fe is lower than that in Figure 5.12.

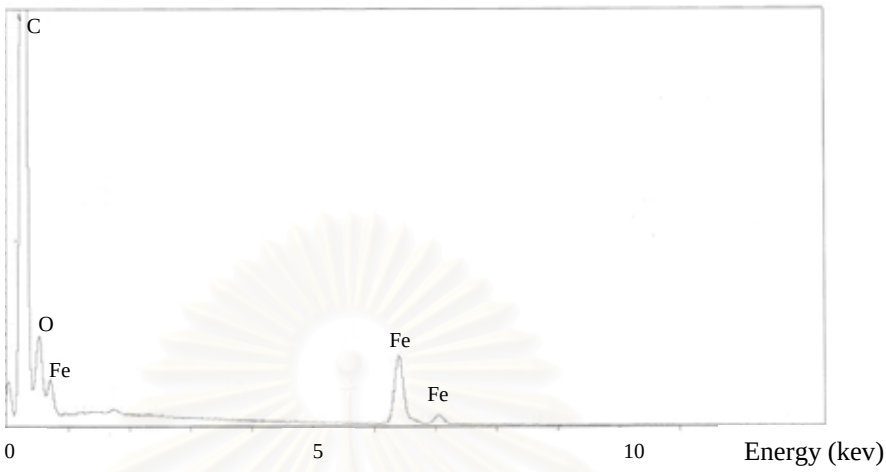

Figure 5.11 EDX analysis of the tip of aligned CNTs from pyrolysis process at 800˚C with molar ratio of 1:1

Figure 5.12 EDX analysis of the CNCs from pyrolysis process at 1050˚C with molar ratio of 1:1

5.1.2.2.2 X-ray Diffraction (XRD) analysis

XRD characterization is performed to further validate the corresponding structure of the core and shell of nanoparticles. The XRD result of the as-synthesized products from ferrocene-naphthalene mixture with molar ratio of 1:1 pyrolysed at 850˚C is shown in Figure 5.13. The diffraction peak at about 26.3˚ can be assigned to the (002) planes of hexagonal graphite structure with an interlayer spacing of 0.34 nm, corresponding to the graphitic interlayer spacing from TEM image. The iron cores are crystalline and exhibit the (110) plane of the fcc-Fe crystal (face-centered cubic) as shown in the Figure 5.9 b) at XRD peak 43.7˚. In addition, it can be seen the others peak from the Figure 5.13 such as: bcc-Fe (110) at 44.7˚, fcc-Fe (200) at 48.8˚. However, it can observe iron carbide (Fe_3C) and iron oxide (Fe_3O_4) with including in the as-grown prepared CNPs.

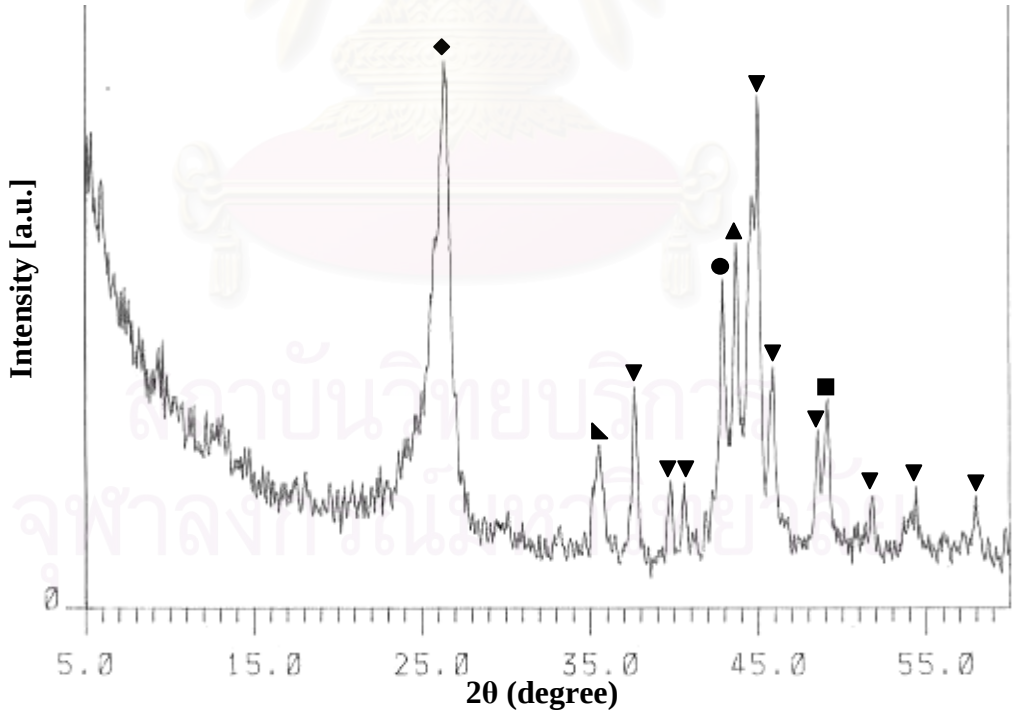

Figure 5.13 XRD pattern of products obtained at 850˚ C with molar ratio of 1:2

◆ (002) Graphite structure (26.3˚) ▲ (110) bcc-Fe (44.7˚)

● (111) fcc Fe (43.7˚) ▼ Fe_3C (iron carbide)

■ (200) fcc-Fe (48.8˚) ◣ Fe_3O_4

The Figure 5.14 shows the XRD results from the prepared CNPs from pyrolysis at 1050˚C. The result shows the structure of obtained CNPs as same as Figure 5.13. It can be found the hexagonal graphite structure and also iron oxide, iron carbide and bcc of fcc of iron form this sample.

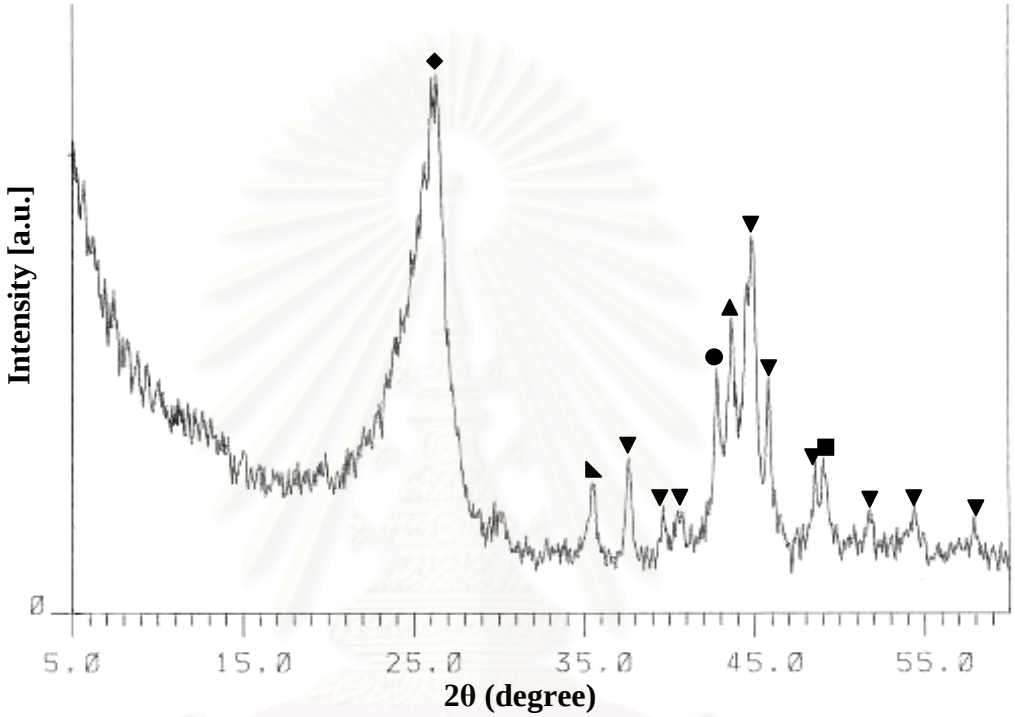

Figure 5.14 XRD pattern of products obtained at 1050˚ C with molar ratio of 1:2

◆(002) Graphite structure (26.3˚) ▲ (110) bcc-Fe (44.7˚)

● (111) fcc Fe (43.7˚) ▼ Fe_3C (iron carbide)

■ (200) fcc-Fe (48.8˚) ◣ Fe_3O_4

It should be noted that the iron particles in the as-grown products are in the form of iron oxide (Fe_3O_4), which is obtained by a reaction of oxygen remained in the process, and in the phase of iron carbide (Fe_3C) and metallic phase of bcc-Fe (110) fcc-Fe (111) and fcc-Fe (200). The well-crystallized graphite could be recognized as higher diffraction peak. However, when the temperature was increased the iron carbide formed was reduced as could be seen in Figures 5.13 and 5.14 as iron carbide peak. It is reported that the formation rate of iron carbides is higher than their decomposition rate at the temperatures below 725 ˚C [20].

5.1.2.3 Mechanism of CNPs formation

It can be accepted that the mechanism of the formation of CNPs induced by iron catalyst involves in decomposition, diffusion and precipitation process. This mechanism can be illustrated in Figure 5.15. First, carbon atoms from naphthalene or/and also ferrocene and iron catalyst precursors will be vaporized after the container of raw material is placed at the previously determined position in the tube reactor. Carbon and iron clusters generated from ferrocene and naphthalene will be carried by a carrier gas to the zone of higher temperature at which the decomposition of the reactive molecules takes place. The decomposition of the gas causes the appearance of free carbons and active iron particles [19], which is important for the formation of carbon nanoparticles.

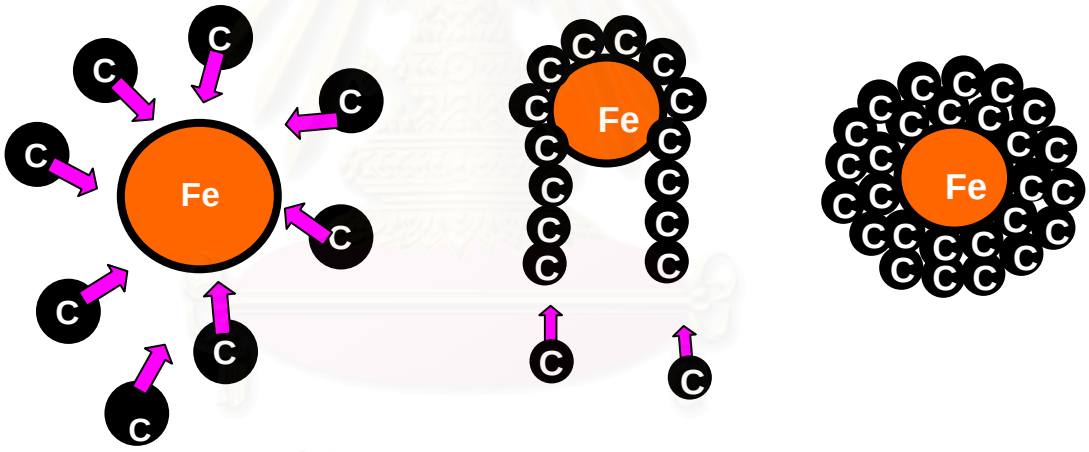

Figure 5.15 Growth mechanisms of CNPs; (a) free carbon with iron catalyst, (b) CNTs formation, (c) CNCs formation

While the iron atoms aggregate to form nanoparticles on the surface of the quartz substrate they behave as seeds for the growth of carbon nanoparticles. Then free carbon atoms will dissolve in or react with the iron particles, resulting in the accumulation of carbon atoms for the formation of graphitic film at the initial stage of the growth. When the dissolution of the carbon reaches its saturation the precipitations of graphite layers will further start. The graphitic layers form rapidly

and enclose the iron nanoparticles, generating a concentric shell of the encapsulated nanoparticle. As the results, CNPs with iron nanoparticles can be obtained and the residue gas will be purged with carrier gas to the atmosphere.

According to this mechanism, it can be suggested that with an increase in temperature the higher diffusion rate of free carbon atoms and the higher reaction rated at the surface of the iron catalysts could be expected. Therefore, an increase in the amount of encapsulation of carbon nanoparticles could be obtained. From SEM analysis, high-quality well-aligned carbon nanotubes were formed between 800 °C and 900 °C. At 850 °C, the highest-quality carbon nanotubes similar to that of Zhang [19] were obtained. On the other hand, at 950˚C or higher temperature the larger amount of CNCs could be observed.

Many reports have proposed some kinetic models of CNPs formation based on the assumption that the rate equation of CNPs can be assumed as a zero order reaction. By employing the Arrhenius equation, one will be able to estimate the rate constant at any other temperature as shown in appendix D. According to Lee's experimental data [23], CNTs formation model can be predicted by using the linear relationship between logarithms of the rate of CNTs formation and $\frac{1}{T}$. Therefore, for carbon nanotubes formation, the rate equation (see appendix D) can be expressed as shown in equation 5.1.

$$r_{CNTs} = 992.27 \cdot e^{\frac{-146.5\times10^{3}}{RT}} \qquad (5.1)$$

For rate of formation of CNCs, it could be assumed the same collision frequency (A value) with CNTs formation because both structures are also carbon cluster. While CNCs has more similar structure to graphite structure compared with CNTs. Therefore, the activation energy of CNCs formation could be assumed from enthalpy change of graphite ($\Delta H_{graphite} = 40.5 \quad {kJ}/{mol}$) which different from the activation energy proposed by Lee [23]. Similarly, for carbon nanocapsules, the rate equation obtained from experimental results is shown as follows,

$$r_{CNCs} = 992.27 \cdot e^{\frac{-40.5\times10^{3}}{RT}} \qquad (5.2)$$

These theoretical analysis reveal that the rate of CNCs formation would be faster enhanced by the increasing temperature because of its lower activation energy. Therefore under the condition of higher temperature, more amounts of CNCs could be synthesized which consistent in previous SEM and TEM results.

5.1.3 Macroscopic analysis

5.1.3.1 Particle size distribution analysis

Dynamic Light Scattering (DLS) has been used for determining particle size distribution of the synthesized CNPs. The as-grown film of CNPs is sampled and dispersed in toluene and then ultrasonicated for 15 minutes. A typical well dispersed sample is characterized for their particle size distribution by ZETASIZER 300HSA as which is shown in Figure 4.10.

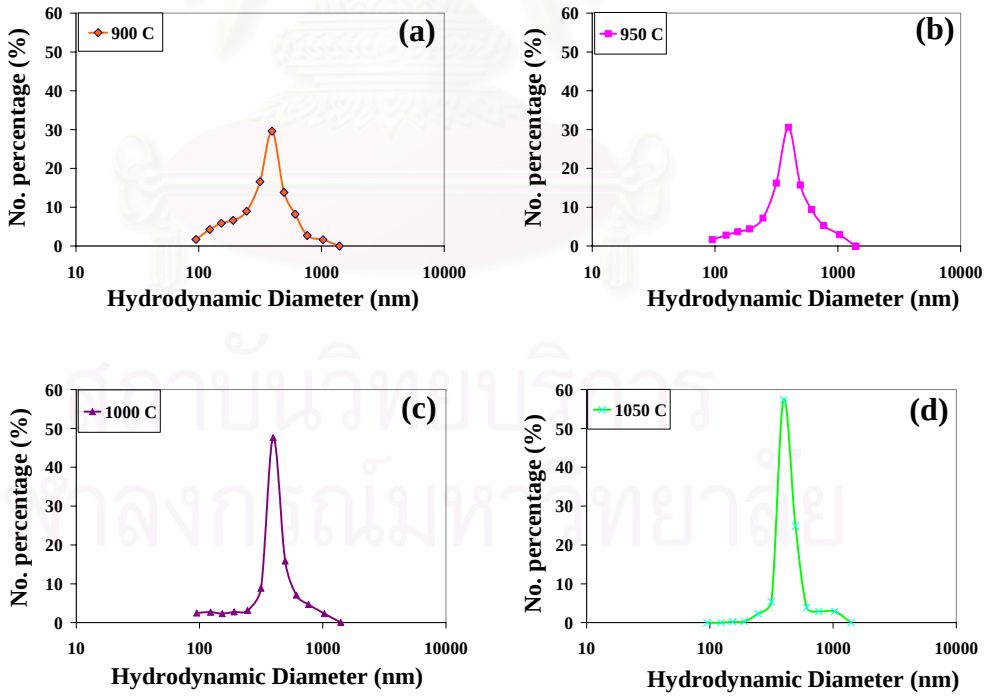

Figure 5.16 Particle size distributions of CNPs obtained from pyrolysis of Naphthalene and Ferrocene with molar ratio of 1:2;
(a) 900˚C, (b) 950˚C, (c) 1000˚C, (d) 1050˚C

Based on experimental results, the hydrodynamic diameter of the obtained CNPs is in a range of 95-1400 nm which a little bit higher than SEM observation due to the agglomeration of the obtained CNPs. With an increase in the temperature the particles size distribution shifts to the range of larger size. According to CNPs formation mechanism discussed previously, it should be noted that iron particles is responsible for the initiation of CNPs formation. Therefore, the CNPs size is dependent on the size of the iron nanoparticle precursors. At higher pyrolysis temperature, the average size of the active catalytic particles becomes larger due to coalescence. Therefore, the larger iron particles consuming more intake of free carbon could lead to CNPs with larger diameters at higher pyrolysis temperature as shown in Figure. 5.16. From these PSDs, dependence of the average hydrodynamic diameter of the obtaineded CNPs on temperature is shown in Figure 5.17. It illustrates that the increasing temperature could result in a linear increase in the larger CNPs.

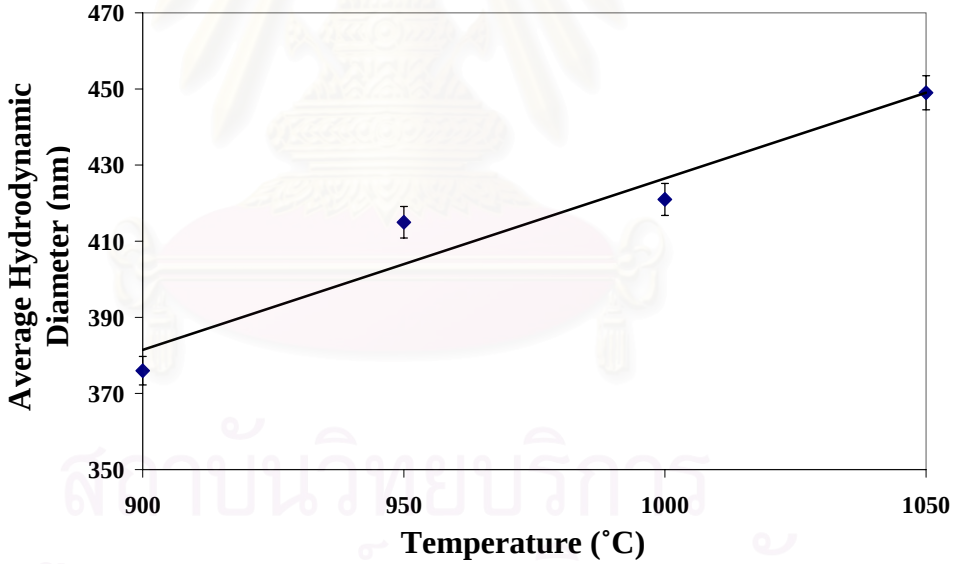

Figure 5.17 Temperature dependence of hydrodynamic diameters of CNPs obtained from pyrolysis of Naphthalene and Ferrocene with mole ratio of 1:2.

5.1.3.2 Raman spectroscopic analysis

The effect of the pyrolysis temperature on the crystallinity of the obtained CNPs has been investigated by Raman spectroscopy as shown in Figure 5.18 below. Theoretically, the crystallinity of carbon nanoparticles could be determined from the

ratio of G peak (1590 cm^{-1}) to D peak (1340 cm^{-1}) obtained from the Raman shift spectrum. When the temperature is increased the crystallinity of the obtained CNPs becomes decreased. This is consistent with the qualitative analysis by microscopic observation (SEM and TEM). With the higher temperature, besides an increase in the presence of CNCs, more amorphous carbon nanoparticles could also be observed.

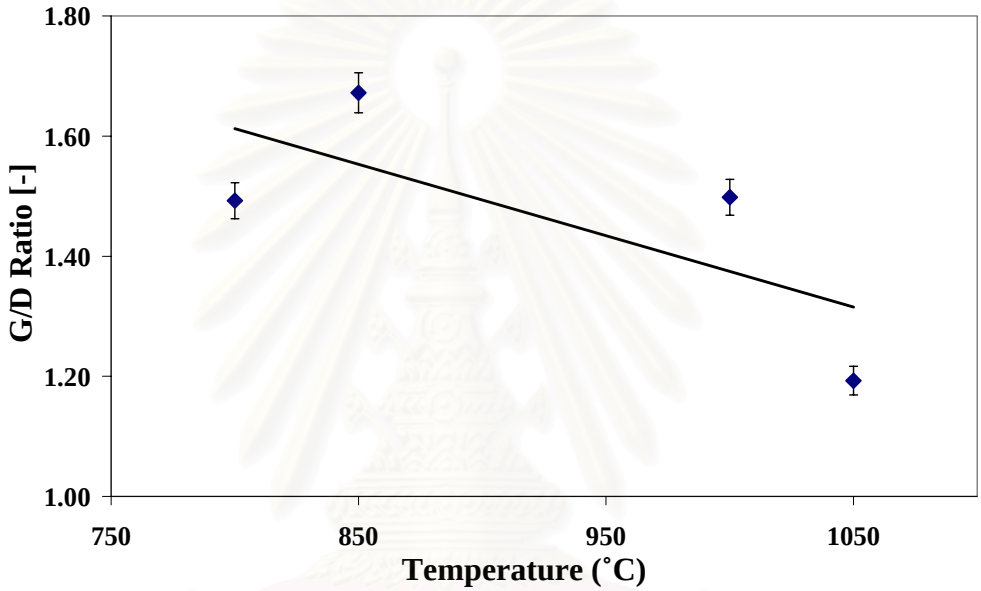

Figure 5.18 G/D ratio of as-grown products characterized by Raman spectroscopy

5.1.3.3 Yield of the obtained nanoparticles

The yield of the obtained products which mainly contain CNPs can be determined from the weight of ferrocene-naphthalene mixture used and the weight of the CNP-rich products as defined in equation 5.3. $M_{recieved}$ is total mass of the as-grown products obtained from pyrolysis and M_{used} is total mass of ferrocene-naphthalene mixture. Interestingly, a small amount of amorphous carbon is also generated in the obtained products CNPs causes the actually yield of CNPs has a little bit dropped. Therefore the methodologies for separating amorphous carbon from desired CNPs is suggested to conduct further in the future.

$$Yield = \frac{M_{recieved}}{M_{used}} \quad (5.3)$$

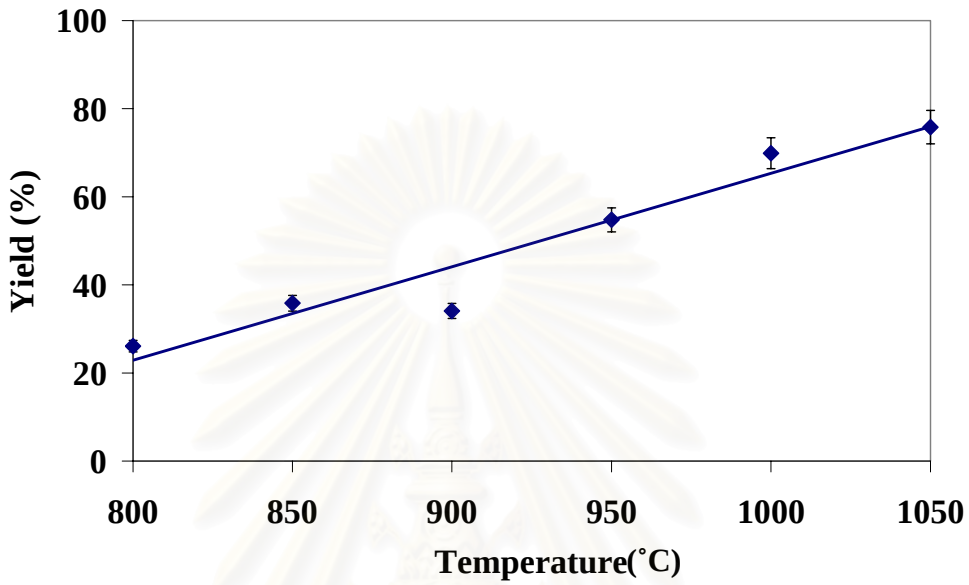

Figure 5.19 Temperature dependence of yield of products with rich CNPs obtained from pyrolysis of ferrocene-naphthalene with1:1 molar ratio

As shown in Figure 5.19, it should be noted that the yield of products with rich CNPs become higher when the temperature is increased. The lower temperature cause the lower yield because when the temperature is low the temperature profile along the tube reactor becomes dropped, leading to higher condensation of naphthalene. Therefore fewer amount of raw material could be utilized in the synthesis.

5.2 Effect of molar ratio of mixture

5.2.1 SEM and TEM analysis

In order to investigate the effect of molar ratio of the Ferrocene and Naphthalene mixture on the morphology of the obtained CNPs, the pyrolysis temperature is kept constant at 1050˚C. As the main objective of research, fraction of naphthalene is increased for the purpose of the increasing carbon atoms engaging in

the nanoparticles synthesis. Since the cost of the pure Naphthalene is lower than that of Ferrocene, the increasing fraction of Naphthalene might result in a decrease in syhthesizing cost. Typical SEM images of the obtained CNPs are shown in Figure 5.20. It could illustrate the change of the product morphology with varying ferrocene to naphthalene mole ratio (F/N) under the same pyrolysis condition. With the increasing molar fraction of Naphthalene more CNTs can be generated. According to the mechanism of nanoparticles formation, it should be noted that once free carbon atoms are continuously and sufficiently supplied to reaction zone CNTs will be preferably grown. Figure 5.20 c) shows that more amount of CNTs could be obtained when 5 moles of Naphthalene is mixed with one mole of Ferrocene.

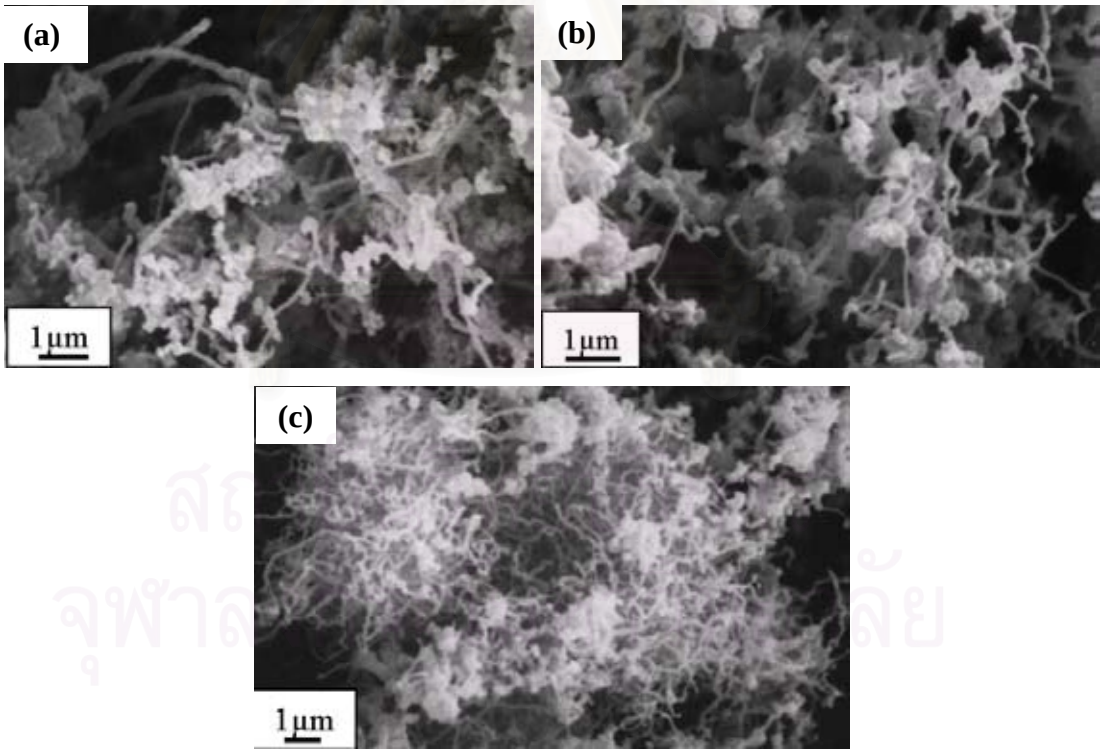

Figure 5.20 SEM images of CNTs at 1050°C in different molar ratio (a) 1:1 molar ratio (b) 1:2 molar ratio (c) 1:5 molar ratio

5.2.2 Particle size analysis

Sampled products are also taken carefully to characterize further by DLS analysis. A typical result is shown in figure 5.21. Though there is some deviation in the average hydrodynamic size of the obtained CNPs, the increasing trend of the average size with respect to the increasing molar fraction of Naphthalene could be observed. Additionally, the temperature dependence of the average size of the CNPs obtained from any molar ratio is also consistent with the previously discussed results.

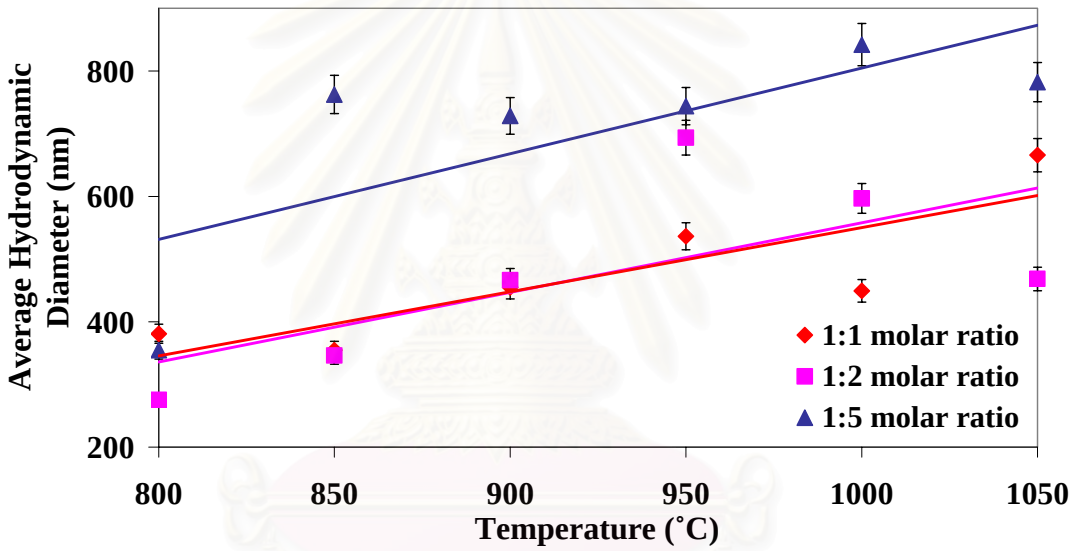

Figure 5.21 Hydrodynamic diameters of CNPs at different molar ratio of mixture

Table 5.1 shows the ratio of free carbon atom to the iron atom theoretically obtained from the complete decomposition of the mixture of each different molar ratio. The ratio of free carbon atom to catalyst (Fe) atom is highest (60:1) at molar ratio of 1:5. With higher number of carbon atom, higher concentration of carbon vapor to be supplied to the reaction zone with the presence of iron atom would be expectable.

Table 5.1 Ratio of carbon atom to iron atom at different molar ratio

Molar ratio of ferrocene:naphthalene (F:N)	Number of carbon atom:iron atom (C:Fe)
1:1	20:1
1:2	30:1
1:5	60:1

5.2.3 Yield of the obtained nanoparticles

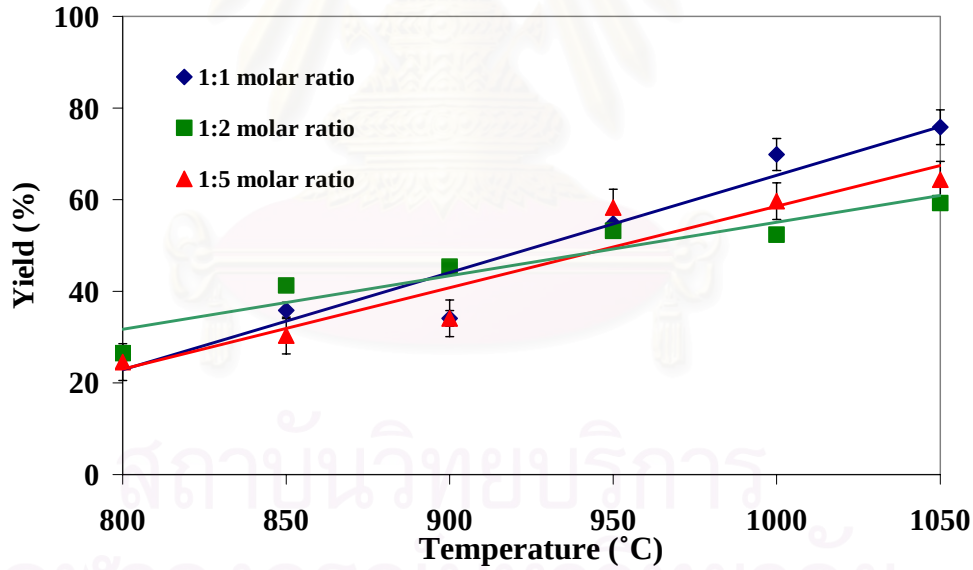

Figure 5.22 Yield of obtained products with rich CNPs at different molar ratio of mixture

Again, the yield of the obtained products can be determined from the weight of ferrocene-naphthalene used and weight of the obtained product (equation 5.3). When using ferrocene-naphthalene mixture with different molar ratio in pyrolysis process, the effect of pyrolysing temperature on the obtained product yield is

illustrated in Figure 5.22. It should be said that the increasing of additional carbon source does not provide any significant difference in the product yield because the initial amount of ferrocene used is the same for every condition. However, more free carbons can be generated during the decomposition of the mixture while the amount of iron catalyst which necessary for the formation of CNPs is still constant. Therefore, when the amount of catalyst is not sufficient, the CNPs cannot be produced further. Furthermore it is found that the higher yield could be found at higher pyrolyzing temperature (as discussed in 5.1.3.3 section).

5.3 Effect of type of the carrier gas

The carrier gas is one of the important variables effecting on the structure of the obtained carbon nanoparticles. Many reports have tried to use in the different kinds of carrier gas, i.e.; hydrogen, argon etc., for conducting on pyrolysis process. It can be accepted that hydrogen is a kind of good alternatives for using as carrier gas which can improve the graphitization for carbon nanoparticles formation. But using of hydrogen gas is risk on the explosion and many problems in safety. The other type is argon gas which can prevent the oxidation of carbon nanoparticles during the process [19]. However, nitrogen gas is one of the inert gas that can prevent the oxidation of iron particles and cheaper than argon or hydrogen gas. Therefore, this research project has used two different carrier gas, nitrogen gas and argon gas, in co-pyrolysis process and study on the structure of obtained nanoparticles. The results for these kinds of carrier gas as follow.

5.3.1 Nitrogen atmosphere

5.3.1.1 Raman spectroscopy analysis

Raman spectroscopy is used to further characterize overall information of the structure and crystallinity of the synthesized CNPs from co-pyrolysis of ferrocene-naphthalene mixture. Raman spectrum of the as-grown of CNPs illustrates two main frequency peaks as shown in Figure 5.23. The first peak indicated G band at 1580

cm^{-1} which associated with the E_{2g} mode (stretching vibrations) in the basal-plane of graphite [20]. The D band at 1340 cm^{-1} has been explained as disorder-induced features due to the finite particle size effect, lattice distortion or amorphous carbon background signals. However, the intensity ratio between G peak and D peak (I_G/I_D) can be indicated the quantity of the good crystallinity of CNTs compared with the amorphous carbon formed.

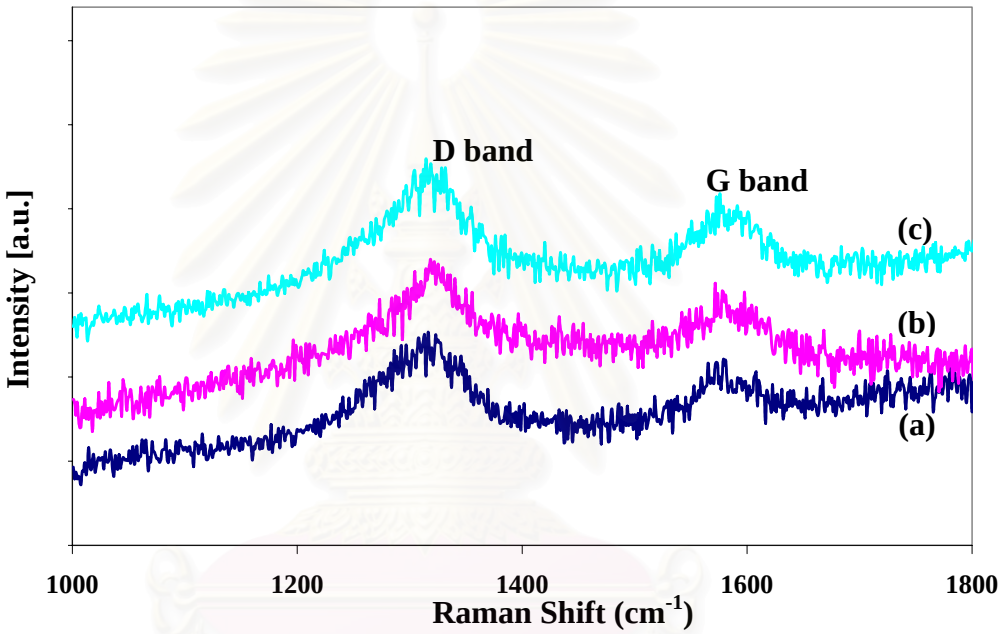

Figure 5.23 Raman Spectroscopy for pyrolysis the mixture under nitrogen atmosphere (1:1 molar ratio); a) 850˚C, b) 950˚C, c) 1050˚C

From the observation, the intensity ratio of I_G/I_D of synthesized CNPs is less than unity. It can be suggested that when pyrolysis has occurred under nitrogen atmosphere so more amorphous can be obtained. With increasing the pyrolysis temperature, the ratio between G peak intensity and D peak intensity (I_G/I_D) becomes decreased. This result shows that when the temperature is increased the amount of CNTs formed also becomes decreased which is consistent with corresponding to the previous discussion. Therefore, the intensity of G peak could be expected to become lowered. The G/D ratio has shown in Figure 5.24.

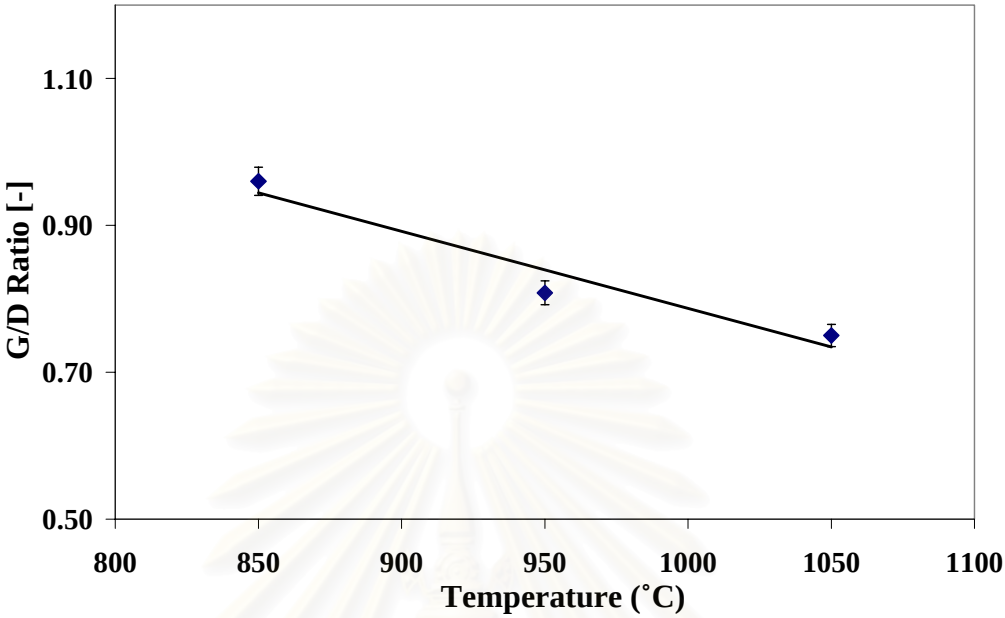

Figure 5.24 G/D ratio of Raman spectroscopy for pyrolysis under nitrogen atmosphere

SWNTs can be obtained when ferrocene and naphthalene mixture was pyrolized under nitrogen atmosphere. However, it is found that the growth process of SWNTs is not clearly understood until now and the growth mechanism of SWNTs needs further research [16]. The Raman spectroscopy was used to characterize the diameter distribution of SWNTs generated. The resonant Raman spectra of SWNTs show two main zones features: radial breathing mode (RBM) band as shown in Figure 5.25 and D, G band as shown in Figure 5.23. From the RBM frequency, ω_{RBM}, the information about SWNTs diameter can be obtained which based on the relation between tube diameter (d in nm) and ω_{RBM} frequency (ω in cm^{-1}) as shown in equation 5.4 [16].

$$d = \frac{254 .61}{\omega} \qquad (5.4)$$

The corresponding diameters of the SWNTs were calculated to be 1.45, 1.16 and 0.93 nm, respectively, which is smaller than TEM observations, probably due to the interaction between the SWNTs in the bundles [16] however the amount of

SWNTs obtained in these conditions is not enough therefore, until now the microscopic pictures of these SWNTs are unavailable.

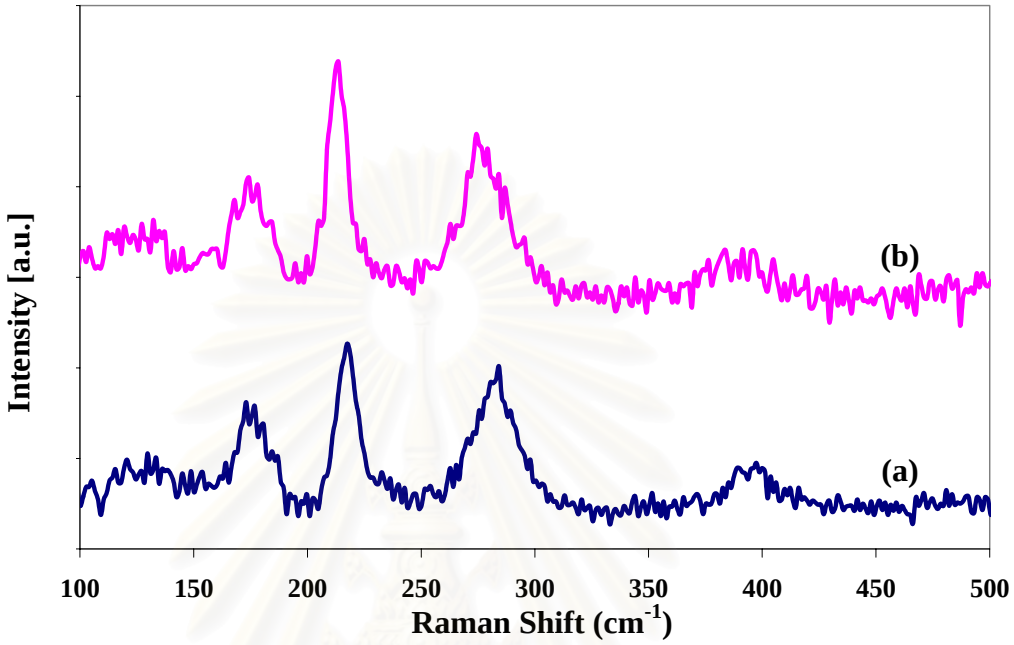

Figure 5.25 Radial Breathing Mode (RBM) for pyrolysis the mixture under nitrogen atmosphere (1 to 1); a) 850˚C, b) 1050˚C

5.3.1.2 Microscopic analysis

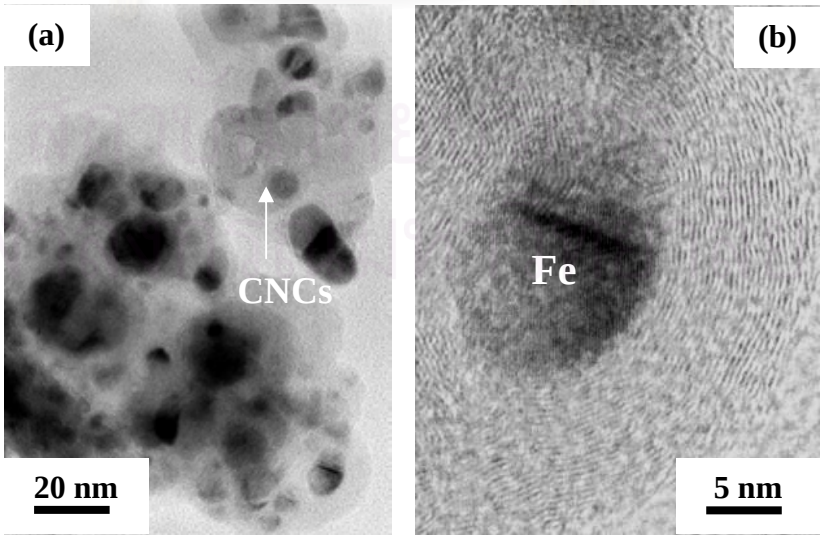

Figure 5.26 TEM of CNCs from pyrolysis at 1050˚C under nitrogen atmosphere (a) Low-magnification, (b) High-magnification

TEM observation of the as-grown products from pyrolysis the ferrocene-naphthalene mixture under nitrogen atmosphere has shown in Figure 5.26. The result has shown the CNCs structure with iron core nanoparticles. The CNCs diameter is between 5-30 nm with graphitic shells around the iron particles. From high-magnification TEM as in Figure 5.26 (b), it can be clearly seen graphene sheets layers about 16 layers. These crystallinity CNPs can be detected by Raman spectroscopy as shown in section 5.3.1.1. However, for the observation of whole prepared CNPs indicated the formation of other impurities like amorphous carbon and the lattice distortion of CNPs which can be detected by D band of Raman result.

5.3.2 Argon atmosphere

5.3.2.1 Raman spectroscopy analysis

The information about structure of carbon shell of CNPs from pyrolysis of ferrocene-naphthalene mixture under argon atmosphere was also obtained from Raman investigation as shown in Figure 5.27. A typical Raman spectra of the obtained CNPs sampled at 1:1 molar ratio of mixture which is characterized by two main peaks centered at 1340 cm^{-1} (D band) and also 1588 cm^{-1} (G band).

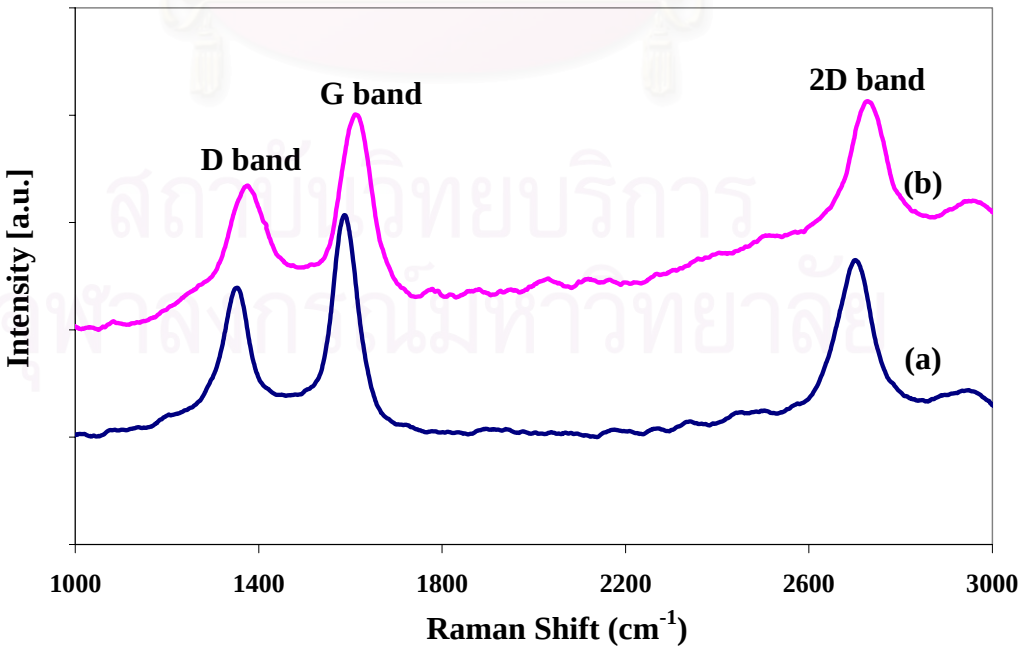

Figure 5.27 Raman Spectroscopy for pyrolysis the mixture under argon atmosphere (1:1 molar ratio); a) 800˚C, b) 1000˚C

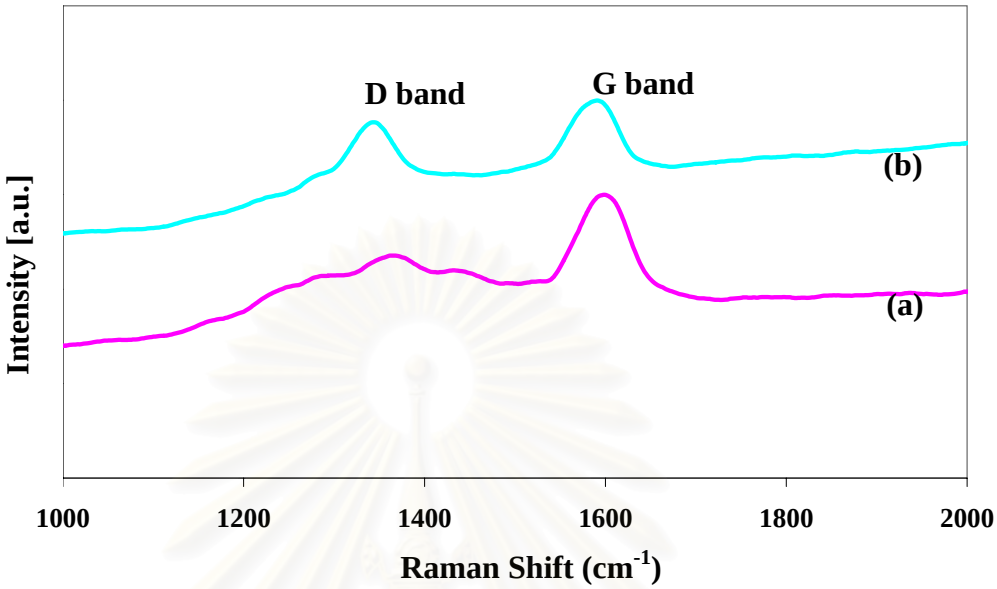

Figure 5.28 Raman Spectroscopy for pyrolysis the mixture under argon atmosphere (1:5 molar ratio); a) 850˚C, b) 1050˚C

From the results, the high peak intensity ratio of I_G/I_D indicates that the as-grown CNPs have good crystallinity of graphene sheet compare with disorder form. The value of I_G/I_D increases from 1.19 to 1.67 as the temperature decreases from 1050˚C to 850˚C. This indicated that at the higher temperature the amount of amorphous is increased which same as the previously discussed about nitrogen gas. From Figure 5.29, the strong peak at ≈ 2700 cm^{-1} can be assigned to the second-harmonic vibration associated with ≈ 1340 cm^{-1}(D-band).

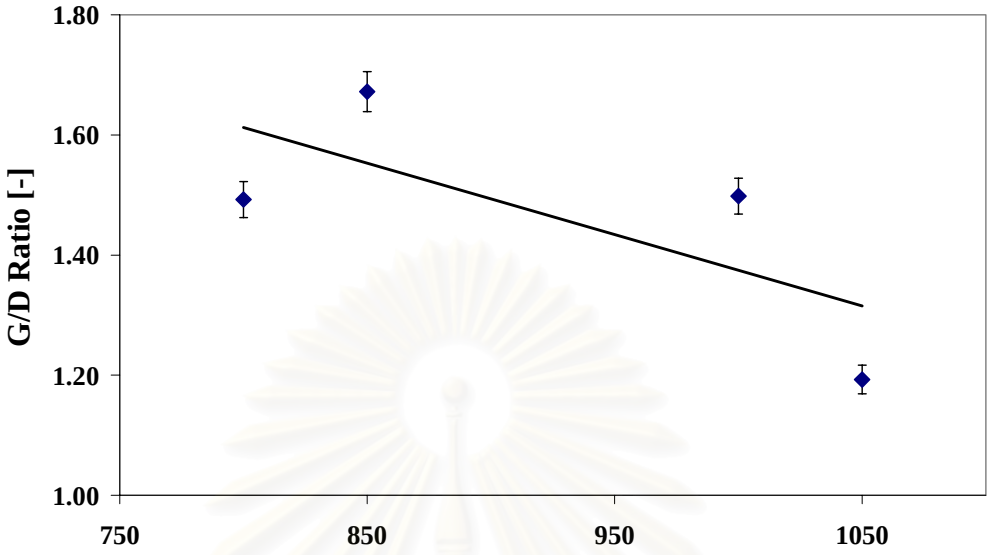

Figure 5.29 G/D Ratio of Raman spectroscopy for pyrolysis under Argon atmosphere

It should be noted that the species of carrier gas can be effect on the crystallinity of the prepared CNPs. Nitrogen gas caused the higher amorphous carbon and also distortion lattice than good crystalline CNPs but argon gas can reduced the amorphous generated. However, both nitrogen gas and argon gas can be provided more amorphous carbon when the pyrolysis temperature is higher.

5.3.2.2 Microscopic analysis

The microscopic analysis of CNPs obtained from pyrolysis under argon atmosphere was investigated by Transmission Electron Microscope. The results have shown as Figure 5.30 and 5.31. From figure 5.30 (a), the low magnification of TEM observation indicated many CNCs formed. The CNCs have the particle size between 10-30 nm with almost spherical shapes and polyhedral shapes. High magnification for CNCs was applied to observe more details as shown in Figure 5.30 (b). The result shows graphene sheets layer about 50 layers around the particles. These graphite sheets indicated the well-construct of CNCs in this condition.

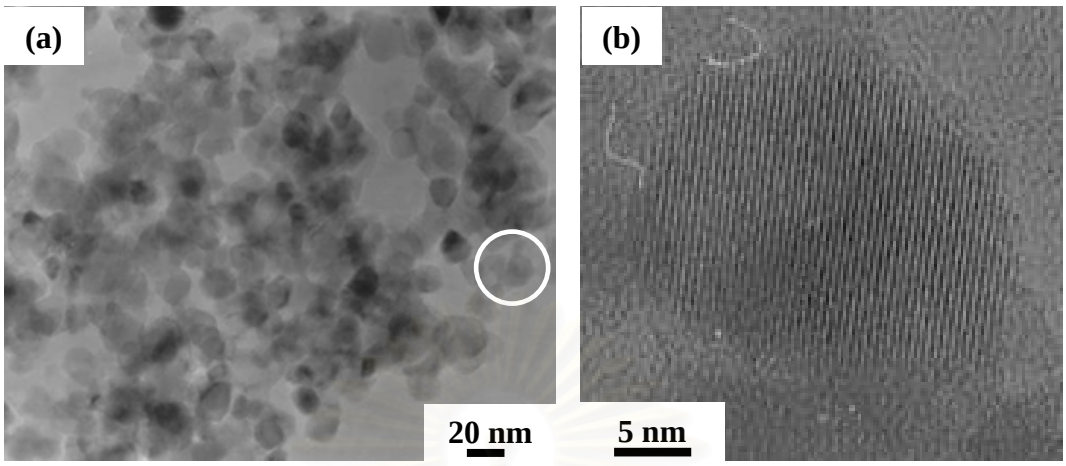

Figure 5.30 TEM images of CNCs at 1050°C under argon atmosphere (a) Low magnification (b) High magnification

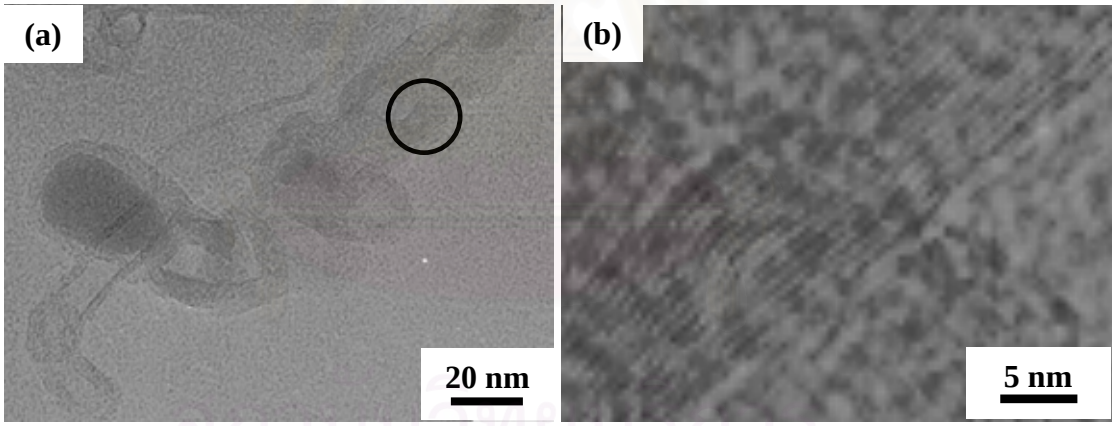

Figure 5.31 TEM image of CNTs at 1050°C under argon atmosphere (a) Low-magnification (b) High-magnification

TEM observation for CNTs has conducted at the same condition. The result has shown in Figure 5.31 CNTs with iron particles in the graphitic shells have shown in Figure 5.31 (a). The figure shows MWCNTs with about 20 nm diameter with 15 graphitic layers. It should be noted that pyrolysis under argon atmosphere could

provide more crystallinity of CNPs. The results are corresponding to the Raman results which G band peak is higher than D band peak.

5.3.3 Yield of the obtained nanoparticles

The effect of the types of carrier gas (nitrogen and argon) on the obtained product yield is illustrated in Figure 5.32. The result illustrates that argon provides more quantities of CNPs than nitrogen gas at low temperature condition and at higher temperature yield of the obtained products from argon is increased more than using nitrogen. It can be explained that argon is an inert gas that hardly reacts with other species. Therefore, when the pyrolysis occurred at higher temperature nitrogen may be reacted with other gas causes the decreased of CNPs yield. The highest yield of 75.81% can be obtained at 1050˚C under argon atmosphere.

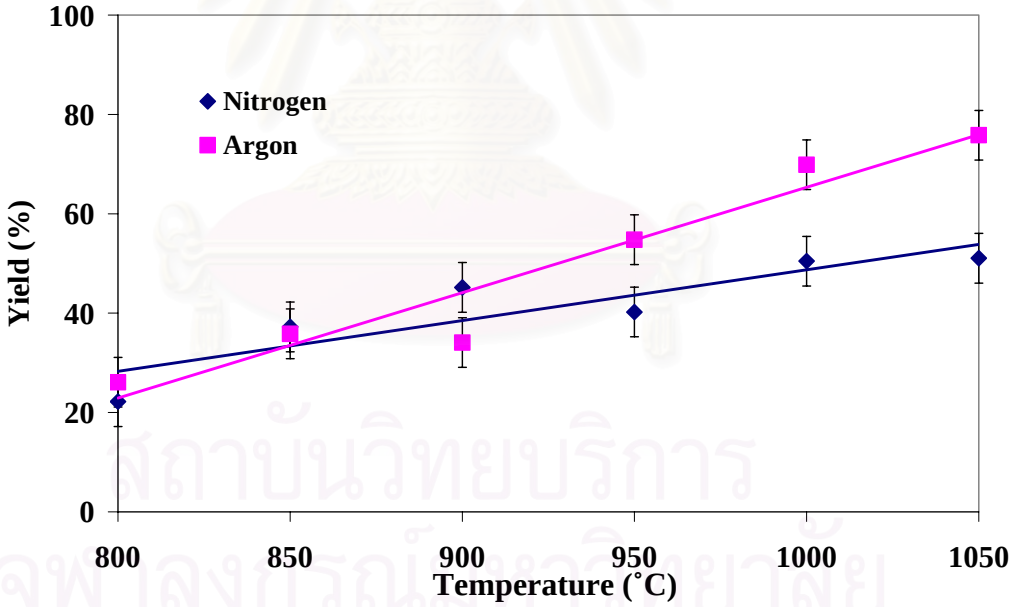

Figure 5.32 Yield of obtained products with rich CNPs at different carrier gas atmosphere

Therefore, using argon atmosphere to accommodate pyrolysis process can prevent the vapors of the mixture undergoing the oxidation reaction. Argon not only prevents the carbon mixture from oxidation but also reduce the quantities of

amorphous carbon from the pyrolysis the results as shown by using Raman spectroscopy as in Figure 5.28. From the results, it can be concluded that CNPs could preferably form under argon atmosphere.

5.4 Effect of the carrier gas flow rate

5.4.1 Flow behavior in the tube

In order to know the flow regime in the tube, Reynolds number of the gas flowing in the tube (equation 5.5) calculated by the following equation.

$$\mathrm{Re} = \frac{\rho v D}{\mu} \tag{5.5}$$

Whereas ρ is density of gas, μ is viscosity and v is superficial velocity of the flowing gas in the tube. The Reynolds number estimation for argon and nitrogen system is shown in Table 5.2. According to this result, it can be implied that all of the flow regimes in the tube are Laminar flow.

Table 5.2 Reynolds number of the gas in the tube

Carrier gas flow rate (cc/min)	Re of flowing Argon	Re of flowing Nitrogen
100	**0.55**	**0.51**
80	**0.44**	**0.41**
50	**0.28**	**0.26**

5.4.1.1 The space time of the carrier gas

When the carrier gas flow rate is increased, the space time for all of the vapors within the system becomes shorter. Assuming the influence of the temperature on the

gas velocity can be neglected, the equation 5.6 is employed to calculate the space time (υ) of the gas in the reactor.

$$\upsilon = \frac{V}{Q} \tag{5.6}$$

Whereas Q is volumetric flow rate and V is the volume of the reactor. The volume of the quartz tube is directly determined from its dimension as shown in equation 5.7.

$$V = \frac{\pi}{4} d^2 \cdot h \tag{5.7}$$

Whereas the inner diameter of quartz tube is 4.1 cm while the length is 65 cm. From this equation, volume of the quartz tube can be calculated about 858.17 cm^3. Table 5.3 summarizes the space time in the reactor at different gas flow rate.

Table 5.3 Space time of the vapor at different flow rate

Carrier gas flow rate (cc/min)	Space time (min)
100	**8.58**
80	**10.73**
50	**17.16**

From the observed phenomena during the pyrolysis process, the ferrocene-naphthalene mixture is normally vaporized within 5 minutes after the process was started. Based on the obtained results from Table 5.3, if the space time of the reactants is more than 5 minutes, it can be implied that all of vapors have enough time to transform to CNPs before they are carried out from the reactor. At the lowest flow

rate of 50 cm^3/min, the longest space time could be achieved to provide the synthesized CNPs with the highest amount compared with other conditions.

5.4.2 Microscopic analysis

Transmission Electron Microscope (TEM) observation of the obtained CNPs at the lowest gas flow rate (50 cc/min) is shown in Figure 5.33. The as-grown CNPs obtained from ferrocene-naphthalene molar ratio of 1:5 at 1050˚C with carried by low argon flowing rate were sampled carefully from 3 different positions in the tube. TEM analysis of the sampled products illustrates the different morphology of the obtained CNPs as shown in the Figure 5.33. At the entrance of the reactor, a large amount of multi-walled structure of CNTs could be formed as shown in Figure 5.33 (a). While at the middle zone of which the highest temperature achieved, MWCNTs with morphology similar to the products collected from the entrance zone could be obtained only fewer amounts as shown in Figure 5.33 (b). Meanwhile, many multi-shelled carbon nanocapsules as shown in Figure 5.33 (c) were synthesized at the downstream zone.

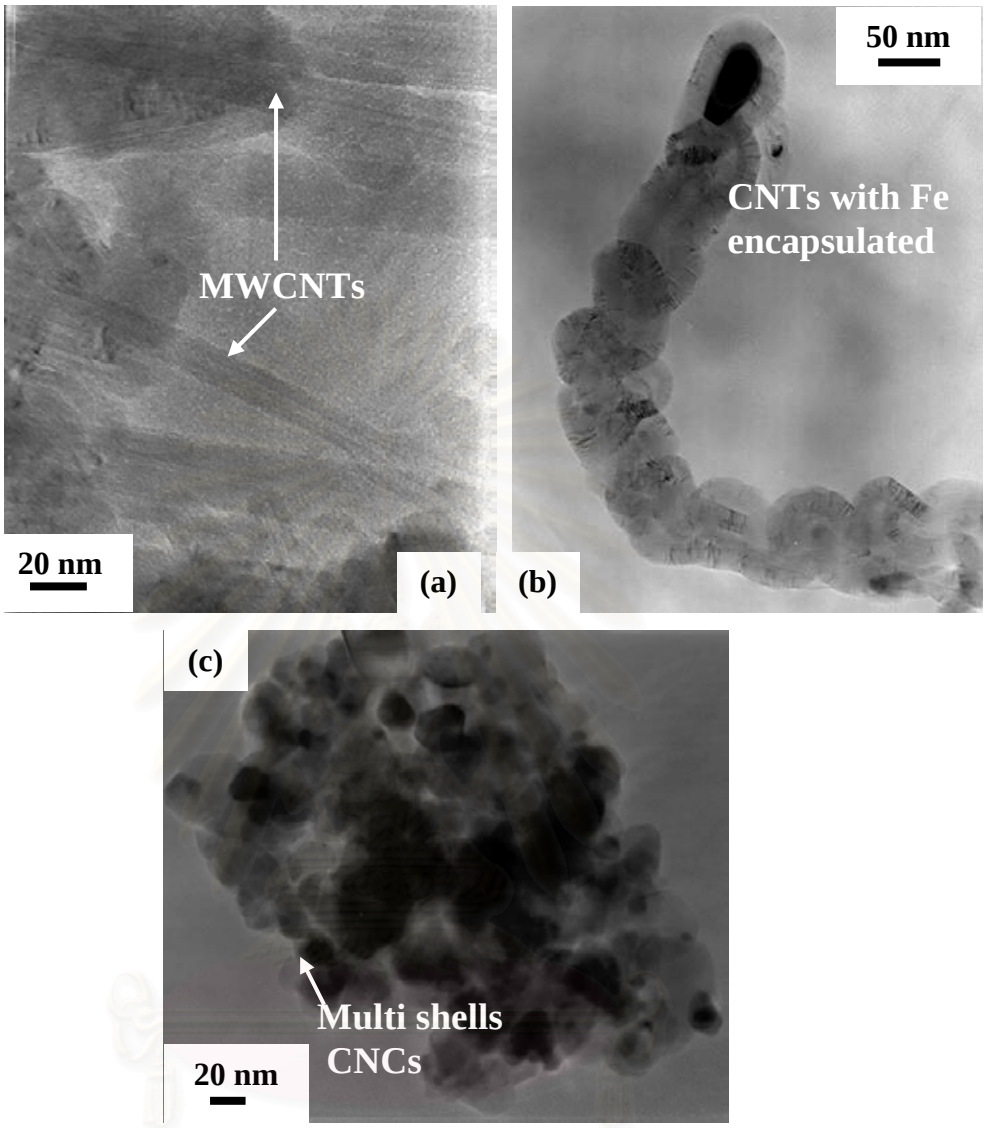

Figure 5.33 TEM of CNPs at different position in the tube
(a) Entrance zone, (b) Middle zone, (c) Downstream zone

Based on the mechanism of the catalytic growth of CNPs as previously discussed in section 5.1.2.3, it should be noted that if the amount of free carbon precursors are not sufficiently supplied to the reaction sites which occupied by Fe nanoparticles, CNTs would not be able to grow. Instead, the CNCs are preferably formed at the downstream of the reactor because most the free carbons precursors generated from ferrocene-naphthalene mixture were almost completely consumed for the formation of CNPs as MWCNTs in the previous zone therefore the remaining free

carbons were not enough for CNTs growth, resulting in the predominant existence of CNCs.

5.4.3 Particle size distribution

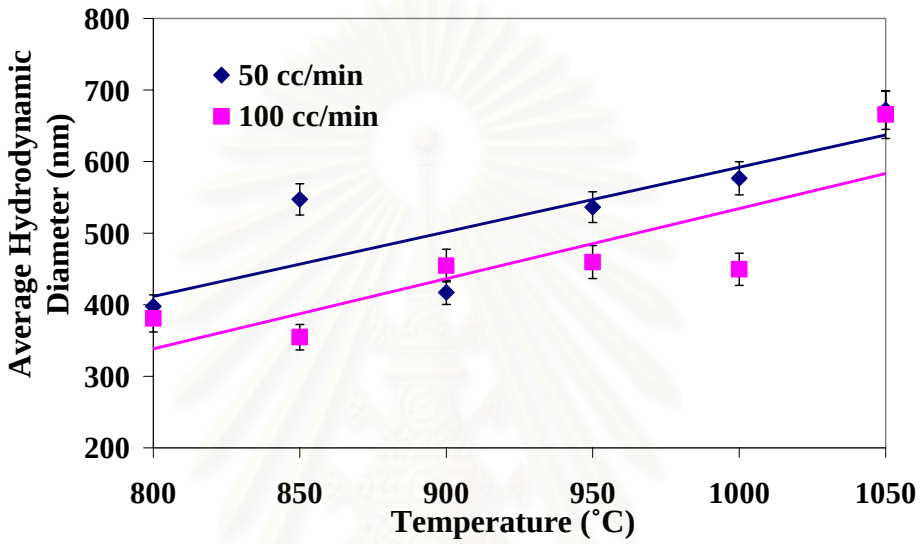

Figure 5.34 Hydrodynamic diameter of CNPs at different carrier gas flow rate

The particles size of CNPs from the different of the carrier gas flow rate investigated by DLS analysis is shown in Figure 5.34. The result shows the tendency of the larger hydrodynamic diameter of CNPs obtained at lower flow rate (50 cc/min). However, the hydrodynamic diameter of CNPs increases when the temperature is raised due to the coalescence of iron core catalyst. At lower carrier gas flow rate, the higher probability of the aggregation of iron nanoparticles can be formed, resulting in the larger diameter of CNPs is obtained.

5.4.4 Yield of the obtained nanoparticles

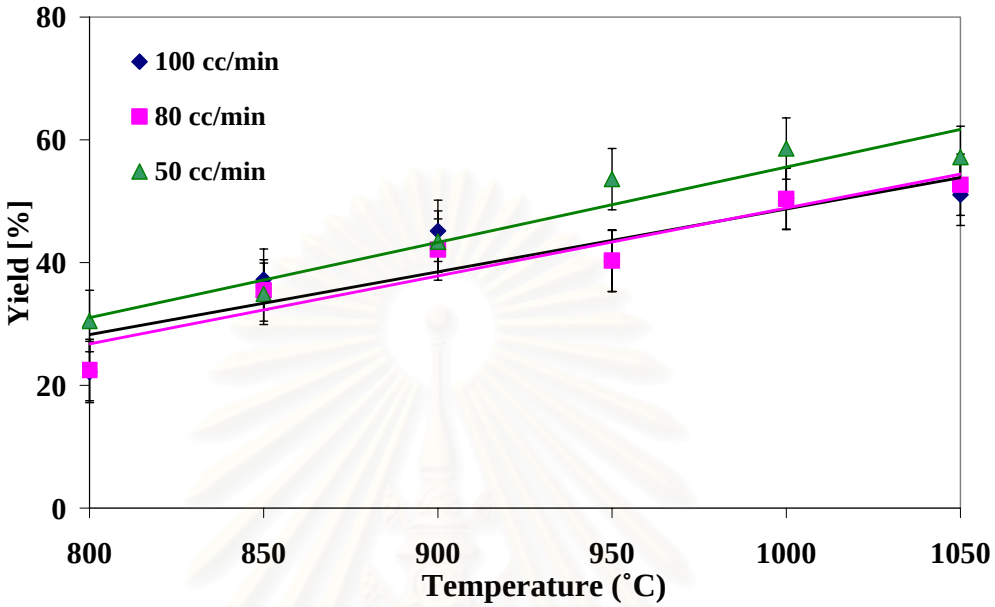

Figure 5.35 Yield of obtained products with rich CNPs at different carrier gas flow rate

From the changing of carrier gas flow rate, the yield of the obtained products which mainly contain CNPs is shown in Figure 5.35. However, the changing of the carrier gas flow rate could effect on the space time required for the CNPs formation. From the result, the quantities of obtained CNPs are not distinctly different while changing gas flow rate. It should be noted that the time required for forming of CNPs from carbon vapors is so fast. Therefore, increasing the space time for the vapor could not be effected on the yield of obtained CNPs.

CHAPTER VI

CONCLUSION AND RECOMMENDATION

6.1 Conclusions

With using of a new additional carbon source, naphthalene, mixed with catalyst precursor, ferrocene, carbon nanoparticles with different structure were synthesized by pyrolysis of the mixture. The main purpose of the present research is to investigate the effect of pyrolysis temperature, molar ratio of mixture, type of carrier gas and carrier gas flow rate on structure, size and morphology of carbon nanoparticles synthesized. From the results, it can be concluded as follows:

6.1.1 Effect of pyrolysis temperature

Pyrolysis temperature is seemed to be a major parameter that affects on the structure of carbon nanoparticles obtained. Carbon nanotubes are prefer to form at low temperature (800˚C-900˚C) and carbon nanocapsules are also form at high temperature(more than 900 ˚C) due to the more reactive of the iron catalyst. At higher pyrolysis temperature, the average size of carbon nanoparticles increases due to coalescence. However, high-quality aligned carbon nanotubes were formed between 800 °C and 900 °C, and at 850 °C, the highest-quality aligned carbon nanotubes were obtained.

6.1.2 Effect of molar ratio of mixture

Number of free carbon is essential for CNPs formation besides pyrolysis temperature. When amount of free carbon is sufficient and continuous supplied to iron catalysts, so CNTs can be produced. On the other hand, if amount of free carbon from carbon source is not enough for tube growth, CNCs can be formed instead of

CNTs. Therefore, number of carbon nanotubes increase with increasing amount of naphthalene thus higher yield can be obtained.

6.1.3 Effect of carrier gas type

The different of carrier gas type used for pyrolysis the mixture can affect on the crystallinity of CNPs received. The two types of carrier gas, nitrogen gas and argon gas, were investigated on the structure and morphology of CNPs received. Nitrogen gas can provide CNPs with amorphous carbons. But using argon gas instead not only can reduced the amorphous formed but also improved the crytallinity of CNPs obtained. However, SWNTs are formed while pyrolysis occurred under nitrogen atmosphere which argon atmosphere cannot provide.

6.1.4 Effect of carrier gas flow rate

Both of the carrier gas types have been studied on the effect of flow rate from 50 -100 cc/min. By increasing the flow rate of carrier gas can decrease the space time of the vapor in the tube which effecting on the particles size of CNPs formed. The particle size distribution of CNPs shows the larger size when lower flow rate was applied. However, the hydrodynamic diameter of CNPs has increased when the temperature is raised due to the coalescence of iron core catalyst. At lower flow rate, the probability of the aggregation of iron nanoparticles is higher than the high flow rate.

6.2 Recommendation for future work

From the experimental results, not only desired products, CNTs and CNCs, are formed but also carbon amorphous and other impurities ie, iron carbide are generated. In order to increase the value added to CNPs obtained, separation methods of these impurities from desired nano-products should be applied such as using acids treatment for separating other amorphous carbon, burning of the products to purge the other impurities etc. For obtaining good crystallinity CNPs hydrogen gas should be used as carrier gas. Hydrogen gas is seemed to be efficient for synthesizing carbon nanoparticles because many reports found that hydrogen gas can improve graphitization process for CNPs. However, the experimental with using hydrogen gas may be risk in explosion during pyrolysis process if the leakage of air occured. For applied to large scale production, growth mechanism of CNPs should be studied for more details.

REFERENCES

[1] P.J.F. Harrris. Carbon Nanotubes and Related Structures. Cambridge: Cambridge University Press (1999).

[2] N. Sano, Tawatchai Charinpanitkul, Tatsuo Kanki, Wiwut Tanthapanichkoon. Controlled synthesis of carbon nanoparticles by arc in water method with forced convective jet. Journal of Applied Physics 96(2004): 645-649.

[3] Y. Kobayashi, H. Nakashima, D. Takagi, Y. Homma. CVD growth of single-walled carbon nanotubes using size-controlled nanoparticle catalyst. Thin Solid Films 464–465 (2004): 286– 289.

[4] M. Zhang, Masako Yudasaka, Sumio Iijima. *Single-wall carbon nanotubes: a high yield of tube through laser ablation of a crude-tube target*, Chemical Physics Letters, 336 (2001): 196-200.

[5] W. D. Zhang , Ying Wen , Jun Li , Guo Qin Xu , Leong Ming Gan. *Synthesis of vertically aligned carbon nanotubes films on silicon wafers by pyrolysis of ethylenediamine*. Thin Solid Films, 422 (2002): 120–125

[6] H. Ago, Satoshi Ohshima, Kazuhito Tsukuagoshi, Masaharu Tsuji, Motoo Yumura. *Formation mechanism of carbon nanotubes in the gas-phase synthesis from colloidal solutions of nanoparticles*. Current Applied Physics (2005): 128–132

[7] C. Emmenegger, J.-M. Bonard, P. Mauron, P. Sudan, A. Lepora,B. Grobety, A. Zuttel, L. Schlapbach. *Synthesis of carbon nanotubes over Fe catalyst on aluminium and suggested growth mechanism*. Carbon 41 (2003): 539–547.

[8] M. C. Schnitzler, Marcela M. Oliveira, Daniel Ugarte, Aldo J.G. Zarbin. *One-step route to iron oxide-filled carbon nanotubes and bucky-onions based on the pyrolysis of organometallic precursors*. Chemical Physics Letters 381 (2003): 541–548.

[9] X. Wang, Yunqi Liu, Daoben Zhu. *Controlled growth of well-aligned carbon nanotubes with large diameter*. Chemical Physics Letters 340 (2001): 419–424.

[10] B.C. Liu, T.J. Lee, S.H. Lee, C.Y. Park, C.J. Lee. *Large-scale synthesis of high-purity well-aligned carbon nanotubes using pyrolysis of iron(II) phthalocyanine and acetylene*. Chemical Physics Letters 377 (2003): 55–59.

[11] N. S. Kim, Yun Tack Lee, and Jeunghee Park. *Vertically Aligned Carbon Nanotubes Grown by Pyrolysis of Iron, Cobalt, and Nickel Phthalocyanines*. *J. Phys. Chem. B* **,** *107*(2003): 9249-9255.

[12] B.C. Satishkumar , A. Govindaraj , C.N.R. Rao. *Bundles of aligned carbon nanotubes obtained by the pyrolysis of ferrocene-hydrocarbon mixtures: role of the metal nanoparticles produced in situ*. Chemical Physics Letters 307 (1999): 158–162.

[13] D.C. Li, Liming Dai, Shaoming Huang, Albert W.H. Mau, Zhong L.Wang. *Structure and growth of aligned carbon nanotube films by pyrolysis*. Chemical Physics Letters 316 (2000): 349–355.

[14] N. Sano , Hiroshi Akazawa , Takeyuki Kikuchi , Tatsuo Kanki. *Separated synthesis of iron-included carbon nanocapsules and nanotubes by pyrolysis of ferrocene in pure hydrogen.* Letters to the Editor Carbon 41 (2003): 2159–2179.

[15] Hq. Hou, Andreas K. Schaper, Frank Weller, and Andreas Greiner. *Carbon Nanotubes and Spheres Produced by Modified Ferrocene Pyrolysis*. Chem. Mater. 2002: 3990-3994.

[16] S. Bai, Feng Li, QuanHong Yang, Hui-Ming Cheng, JinBo Bai. *Influence of ferrocene/benzene mole ratio on the synthesis of carbon nanostructures*. Chemical Physics Letters, 376 (2003): 83–89.

[17] M. Endo , Y.A. Kim , T. Takeda , S.H. Hong , T. Matusita , T. Hayashi , M.S. Dresselhaus. *Structural characterization of carbon nanofibers obtained by hydrocarbon pyrolysis*. Carbon 39 (2001): 2003–2010.

[18] S. Tomita, Masahiro Hikita, Minoru Fujii, Shinji Hayashi, Keiichi Yamamoto. *A new and simple method for thin graphitic coating of magnetic-metal nanoparticles*. Chemical Physics Letters 316 (2000): 361–364.

[19] H. Zhang, Erjun Liang, Pei Ding, Mingju Chao. *Layered growth of aligned carbon nanotube arrays by pyrolysis*. Physica B 337 (2003): 10–16.

[20] Y. Lu, Zhenping Zhu, Zhenyu Liu. *Carbon-encapsulated Fe nanoparticles from detonation-induced pyrolysis of ferrocene*. Carbon 43 (2005): 369–374.

[21] H. Tokoro, Shigeo Fujii, Takeo Oku. *Iron nanoparticles coated with graphite nanolayers and carbon nanotube.* Diamond and Related Materials (2004): 1270–1273.

[22] D.C. Li, Liming Dai, Shaoming Huang, Albert W.H. Mau, Zhong L. Wang. *Structure and growth of aligned carbon nanotube films by pyrolysis*. Chemical Physics Letters 316 (2000): 349–355.

[23] Y. T. Lee, Nam Seo Kim, Jeunghee Park, Jae Beom Han,Young Sang Choi, Hyun Ryu, Hwack Joo Lee. *Temperature-dependent growth of carbon nanotubes by pyrolysis of ferrocene and acetylene in the range between 700 and 1000^{o}C*. Chemical Physics Letters 372 (2003): 853–859.

[24] A. Gorbunov, O. Jost, W. Pompe, A. Graff. *Solid–liquid–solid growth mechanism of single-wall carbon nanotubes*. Carbon 40 (2002): 113–118.

[25] X.X. Zhang, G.H Wen, Shaoming Huang, Liming Dai, Ruiping Gao, Zhong L. Wang. *Magnetic properties of Fe nanoparticles trapped at the tips of the aligned carbon nanotubes*. Letter to the Editor Journal of Magnetism and Magnetic Materials (2001): L9–L12.

[26] M. Terrones, Carbon nanotubes: synthesis and properties, electronic devices and other emerging applications.

APPENDICES

APPENDIX A

Publication of the research

Publication

1. Proceeding of the international conference on Smart Materials (Smart/Intelligent Materials and Nanotechnology), Chiang Mai Thailand 1-3 Dec. 2004, Page 188-190.

APPENDIX B

Experimental Results

1:1 molar ratio

Parameters	Before			After		
Argon gas	Ferrocene wg.	Naphthalene wg.	Bottle Weight	Bottle Weight	net weight	**yield (Cal.)**
1:1 mole ratio [100]						
800 c	0.2804	0.1938	11.2788	11.4025	0.1237	26.09
850 c	0.2804	0.1938	11.4402	11.6101	0.1699	35.83
900 c	0.2804	0.1938	11.6481	11.8097	0.1616	34.08
950 c	0.2804	0.1938	11.1604	11.4201	0.2597	54.77
1000 c	0.2804	0.1938	11.0582	11.3895	0.3313	69.86
1050 c	0.2804	0.1938	11.3089	11.6684	0.3595	75.81
1:1 mole ratio [80]						
800 c	0.2804	0.1938	11.3088	11.4333	0.1245	26.25
850 c	0.2804	0.1938	11.1402	11.3021	0.1619	34.14
900 c	0.2804	0.1938	11.2281	11.4022	0.1741	36.71
950 c	0.2804	0.1938	11.1554	11.3343	0.1789	37.73
1000 c	0.2804	0.1938	11.4232	11.6576	0.2344	49.43
1050 c	0.2804	0.1938	11.2589	11.5363	0.2774	58.50
1:1 mole ratio [50]						
800 c	0.2804	0.1938	11.5475	11.6721	0.1246	26.28
850 c	0.2804	0.1938	11.5809	11.7534	0.1725	36.38
900 c	0.2804	0.1938	11.6373	11.8223	0.185	39.01
950 c	0.2804	0.1938	11.3384	11.5835	0.2451	51.69
1000 c	0.2804	0.1938	11.3419	11.6235	0.2816	59.38
1050 c	0.2804	0.1938	11.1276	11.4098	0.2822	59.51

1:2 molar ratio

Parameters	Before			After		
Argon gas	Ferrocene wg.	Naphthalene wg.	Bottle Weight	Bottle Weight	net weight	**yield (Cal.)**
1:2 mole ratio [100]						
800 c	0.2804	0.3864	11.3523	11.529	0.1767	26.50
850 c	0.2804	0.3864	11.4012	11.6764	0.2752	41.27
900 c	0.2804	0.3864	11.6643	11.9667	0.3024	45.35
950 c	0.2804	0.3864	11.1669	11.5216	0.3547	53.19
1000 c	0.2804	0.3864	11.5419	11.8908	0.3489	52.32
1050 c	0.2804	0.3864	11.3946	11.7896	0.395	59.24
1:2 mole ratio [80]						
800 c	0.2804	0.3864	11.4651	11.6578	0.1927	28.90
850 c	0.2804	0.3864	11.3204	11.5553	0.2349	35.23
900 c	0.2804	0.3864	11.7751	12.0852	0.3101	46.51
950 c	0.2804	0.3864	11.4459	11.8205	0.3746	56.18
1000 c	0.2804	0.3864	11.6141	12.0037	0.3896	58.43
1050 c	0.2804	0.3864	11.5394	11.9423	0.4029	60.42
1:2 mole ratio [50]						
800 c	0.2804	0.3864	11.6011	11.8044	0.2033	30.49
850 c	0.2804	0.3864	11.4556	11.6883	0.2327	34.90
900 c	0.2804	0.3864	11.2527	11.5422	0.2895	43.42
950 c	0.2804	0.3864	11.6158	11.9732	0.3574	53.60
1000 c	0.2804	0.3864	11.1148	11.5054	0.3906	58.58
1050 c	0.2804	0.3864	11.2852	11.6666	0.3814	57.20

1:5 molar ratio

Parameters	Before			After		
Argon gas	Ferrocene wg.	Naphthalene wg.	Bottle Weight	Bottle Weight	net weight	**yield (Cal.)**
1:5 mole ratio [100]						
800 c	0.2804	0.9659	11.5537	11.8596	0.3059	24.54
850 c	0.2804	0.9659	11.3087	11.6868	0.3781	30.34
900 c	0.2804	0.9659	11.4648	11.8897	0.4249	34.09
950 c	0.2804	0.9659	11.2895	12.0157	0.7262	58.27
1000 c	0.2804	0.9659	11.2716	12.0154	0.7438	59.68
1050 c	0.2804	0.9659	11.3021	12.1041	0.802	64.35
1:5 mole ratio [80]						
800 c	0.2804	0.9659	11.3935	11.7534	0.3599	28.88
850 c	0.2804	0.9659	11.3165	11.8063	0.4898	39.30
900 c	0.2804	0.9659	11.4381	11.9267	0.4886	39.20
950 c	0.2804	0.9659	11.3099	11.8892	0.5793	46.48
1000 c	0.2804	0.9659	11.1012	11.8304	0.7292	58.51
1050 c	0.2804	0.9659	11.7258	12.5313	0.8055	64.63
1:5 mole ratio [50]						
800 c	0.2804	0.9659	11.3573	11.6967	0.3394	27.23
850 c	0.2804	0.9659	11.2844	11.8295	0.5451	43.74
900 c	0.2804	0.9659	11.5531	12.0534	0.5003	40.14
950 c	0.2804	0.9659	11.4052	12.0126	0.6074	48.74
1000 c	0.2804	0.9659	11.4288	12.1152	0.6864	55.08
1050 c	0.2804	0.9659	11.3075	12.0755	0.768	61.62

1:1 molar ratio

Parameters	Before			After		
Nitrogen gas	Ferrocene wg.	Naphthalene wg.	Bottle Weight	Bottle Weight	net weight	**yield (Cal.)**
1:1 mole ratio [100]						
800 c	0.2804	0.1938	11.5909	11.6961	0.1052	22.18
850 c	0.2804	0.1938	11.4548	11.6314	0.1766	37.24
900 c	0.2804	0.1938	11.3839	11.5981	0.2142	45.17
950 c	0.2804	0.1938	11.2436	11.4344	0.1908	40.24
1000 c	0.2804	0.1938	11.3542	11.5935	0.2393	50.46
1050 c	0.2804	0.1938	11.4423	11.6844	0.2421	51.05
1:1 mole ratio [80]						
800 c	0.2804	0.1938	11.491	11.5977	0.1067	22.50
850 c	0.2804	0.1938	11.4156	11.5838	0.1682	35.47
900 c	0.2804	0.1938	11.4711	11.6708	0.1997	42.11
950 c	0.2804	0.1938	11.7972	11.9884	0.1912	40.32
1000 c	0.2804	0.1938	11.7088	11.9477	0.2389	50.38
1050 c	0.2804	0.1938	11.2655	11.5153	0.2498	52.68
1:1 mole ratio [50]						
800 c	0.2804	0.1938	11.5708	11.6801	0.1093	23.05
850 c	0.2804	0.1938	11.4314	11.5921	0.1607	33.89
900 c	0.2804	0.1938	11.0569	11.2477	0.1908	40.24
950 c	0.2804	0.1938	11.5366	11.7533	0.2167	45.70
1000 c	0.2804	0.1938	11.4134	11.6322	0.2188	46.14
1050 c	0.2804	0.1938	11.3345	11.5773	0.2428	51.20

1:2 molar ratio

Parameters	Before			After		
	Ferrocene wg.	Naphthalene wg.	Bottle Weight	Bottle Weight	net weight	**yield (Cal.)**
Nitrogen gas						
1:2 mole ratio [100]						
800 c	0.2804	0.3864	11.7247	11.8834	0.1587	23.80
850 c	0.2804	0.3864	11.4512	11.7333	0.2821	42.31
900 c	0.2804	0.3864	11.542	11.8095	0.2675	40.12
950 c	0.2804	0.3864	11.4905	11.8164	0.3259	48.88
1000 c	0.2804	0.3864	11.3095	11.6574	0.3479	52.17
1050 c	0.2804	0.3864	11.8432	12.2076	0.3644	54.65
1:2 mole ratio [80]						
800 c	0.2804	0.3864	11.1893	11.3559	0.1666	24.99
850 c	0.2804	0.3864	11.2363	11.4983	0.262	39.29
900 c	0.2804	0.3864	11.4874	11.8029	0.3155	47.32
950 c	0.2804	0.3864	11.5664	11.8965	0.3301	49.51
1000 c	0.2804	0.3864	11.3021	11.6488	0.3467	51.99
1050 c	0.2804	0.3864	11.5384	11.9084	0.37	55.49
1:2 mole ratio [50]						
800 c	0.2804	0.3864	11.4161	11.6143	0.1982	29.72
850 c	0.2804	0.3864	11.5604	11.8584	0.298	44.69
900 c	0.2804	0.3864	11.379	11.6645	0.2855	42.82
950 c	0.2804	0.3864	11.4802	11.8243	0.3441	51.60
1000 c	0.2804	0.3864	11.6276	11.9866	0.359	53.84
1050 c	0.2804	0.3864	11.3039	11.7055	0.4016	60.23

1:5 molar ratio

Parameters	Before			After		
	Ferrocene wg.	Naphthalene wg.	Bottle Weight	Bottle Weight	net wieght	**yield (Cal.)**
Nitrogen gas						
1:5 mole ratio [100]						
800 c	0.2804	0.9659	11.2671	11.5673	0.3002	24.09
850 c	0.2804	0.9659	11.8159	12.3341	0.5182	41.58
900 c	0.2804	0.9659	11.5386	12.0461	0.5075	40.72
950 c	0.2804	0.9659	11.5556	12.1464	0.5908	47.40
1000 c	0.2804	0.9659	11.6246	12.1983	0.5737	46.03
1050 c	0.2804	0.9659	11.6031	12.3465	0.7434	59.65
1:5 mole ratio [80]						
800 c	0.2804	0.9659	11.4321	11.7224	0.2903	23.29
850 c	0.2804	0.9659	11.7855	12.2954	0.5099	40.91
900 c	0.2804	0.9659	11.2053	11.6745	0.4692	37.65
950 c	0.2804	0.9659	11.5563	12.1544	0.5981	47.99
1000 c	0.2804	0.9659	11.6944	12.3129	0.6185	49.63
1050 c	0.2804	0.9659	11.5649	12.3043	0.7394	59.33
1:5 mole ratio [50]						
800 c	0.2804	0.9659	11.5246	11.8242	0.2996	24.04
850 c	0.2804	0.9659	11.5756	12.0861	0.5105	40.96
900 c	0.2804	0.9659	11.6879	12.2141	0.5262	42.22
950 c	0.2804	0.9659	11.4375	12.0529	0.6154	49.38
1000 c	0.2804	0.9659	11.5299	12.2247	0.6948	55.75
1050 c	0.2804	0.9659	11.6346	12.3912	0.7566	60.71

APPENDIX C

Carbon nanotubes Applications

Carbon nanotube applications

To date, various prototype electronic devices have been developed using single- and multiwalled carbon nanotubes. In the following sections, some applications that could result in nanodevices in the near future are briefly described.

1. Field emission sources

Electrons can be easily emitted from carbon nanotube tips when a potential is applied between a carbon nanotube surface and an anode.Based on this principle, both SWNTs and MWNTs have proved advantageous in the fabrication of different types of efficient field emission sources (Fig.1). Some examples include: flat panel displays, intense light sources or bright lamps and X-ray sources. Some clear advantages of using carbon nanotubes as electron emission devices are:

- stable field emission over prolonged time periods
- long lifetimes of the components
- low emission threshold potentials
- high current densities
- absence of ultrahigh vacuum

In particular, current densities as high as 4 A cm^{-2} have been achievable.

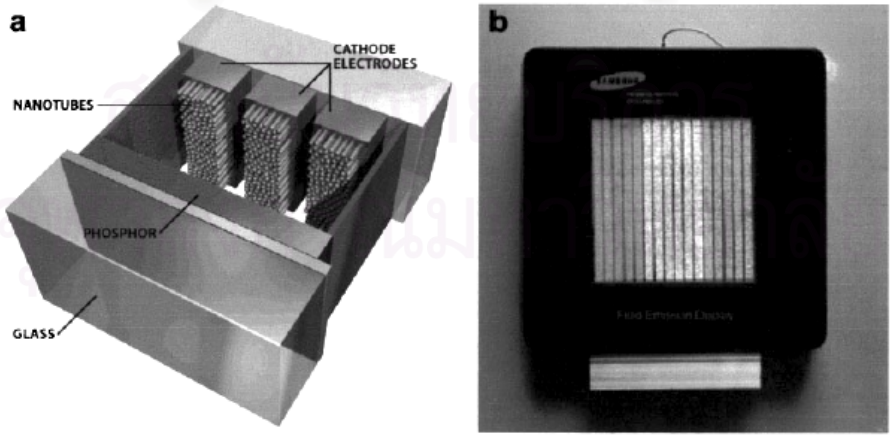

Figure 1 Applications of carbon nanotubes as field emission sources
a) Flat panel display using carbon nanotubes as emission sources (Rotman D.Technology Review, March 2002, 38–45); b) Nanotube display using SWNTs as emission sources produced by Samsung-Korea (courtesy Samsung)

The advantages of carbon nanotube screens over liquid crystal displays are based upon low power consumption, intense brightness, wider viewing angle, fast rate response and a wider operating temperature range. Samsung (Korea) has produced low cost prototypes of commercial nanotube colour displays that can play moving images and, in early 2005, intend to launch on the market TV screens based on carbon nanotubes (Fig.1b). Other electronic companies also intend to release commercial TV screens made of nanotubes in the year 2005. Alternatively, prototypes of carbon nanotube lamps, which could be cheap to manufacture, have exhibited long lifetimes (8000 h), and high efficiency for the color green. The generation of X-rays can also be achieved if metal targets replace the phosphor screen and the accelerating voltage is larger. The generated X-rays have now been used to image human bones.

2. Lithium ion batteries

Lithium is an alkali metal, which donates electrons very easily to form Li^+, and has proved to be extremely important for the fabrication of lightweight and energy efficient batteries. In lithium ion batteries using graphite-like materials, it is possible to intercalate lithium ions within graphite-like structures, so that Li^+ migrates from a graphitic anode to the cathode (usually $LiCoO_2$, $LiNiO_2$ and $LiMn_2O_4$). The theoretical lithium storage capacity in graphite is 372 mA h g^{-1}(LiC_6), and the charge and discharge phenomena in these batteries are based upon the Li^+ intercalation and de-intercalation (Fig. 2). Li^+ based batteries (using graphite-like carbon within the anode) are so far the best energy storage instruments used for assisting portable electronic devices.

The Japanese Company, Sony, was the first company to commercialise such batteries in the 1990s, and at present this technology is used in portable computers, mobile telephones, digital cameras, etc. M. Endo is considered as one of the pioneers in using VGCFs instead of graphite; with his colleagues, he demonstrated that the operation of the battery could be enhanced further. Subsequently, his group proved that boron-doped VGCFs and nanofibres are by far superior when compared to any other carbon source present in the graphitic anode. This may be due to the fact that the population of lithium ions has stronger affinity in the boron-doped sites, thus resulting

in higher energy storage of the battery due to an increase in the cycle characteristics. Nitrogen-doped carbon nanotubes and nanofibres have also shown efficient reversible lithium storage (480 mA h g^{-1}); much higher when compared to commercial carbon materials used for Liz batteries (330 mA h g^{-1}).

Arrays of aligned MWNTs of carbon (pyrolytically grown) could also be used in the anode fabrication for Liz batteries, and the intercalation capacity (490 mA h g^{-1}) is double that of standard carbon. In contrast, highly crystalline MWNTs produced using arc discharge techniques (with closed end caps) revealed a much lower reversible capacity (125 mA h g^{-1}).Other authors have achieved a high electrochemical charging capacity of 800 mA h g^{-1} when using purified SWNTs in Ni–MH batteries. It is also possible to fabricate V2O5–SWNT electrodes that were found to exhibit specific capacities in excess of 400 mA h g^{-1} at high discharge rates and retained this level of capacity on cycling.

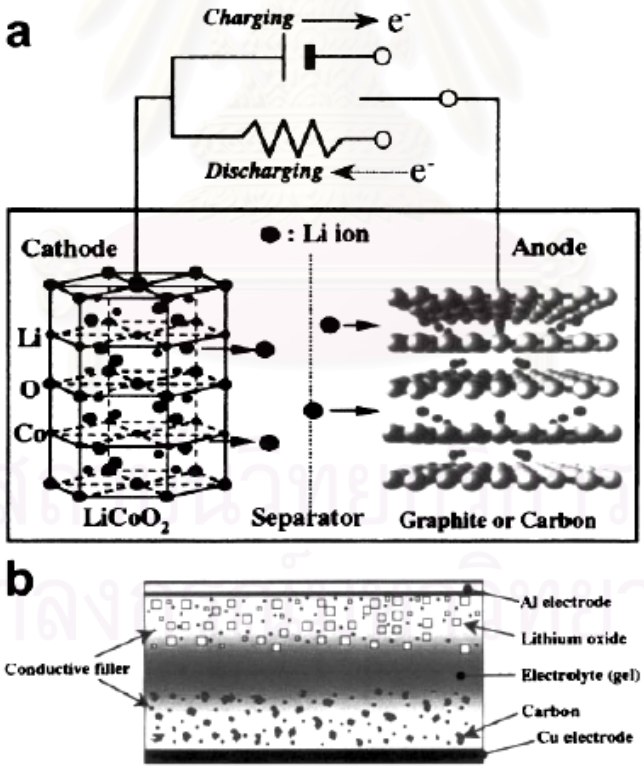

Figure 2 Operation of Li ion batteries (courtesy M. Endo); a) Mechanism for charging–discharging occurring in Li ion secondary batteries; b) Configuration of polymer electrode used in Li ion batteries

3. Molecular sensors

Lieber's group was the first to demonstrate that it is possible to sense functional chemical groups attached at the nanotube ends using chemical force microscopy (CFM). Subsequently, Dai and colleagues were the first to carry out toxic gas sensing experiments using SWNT circuits and pellets. These authors were able to detect parts per million (ppm) of NO_2 or NH_3, by observing strong and drastic transport changes in the SWNT material.36 Almost simultaneously, Collins and co-workers noted that SWNTs were also extremely sensitive to air and vacuum, by observing large variations in the electrical resistance of the SWNT samples. Varghese and colleagues demonstrated that MWNTs could also be used as efficient sensors for NH_3, H_2O, CO, and CO_2. In 2002, highly sensitive and fastresponsive microwave resonant sensors for detecting NH_3 were prepared using either SWNTs or MWNTs.

More recently, films of aligned CNx nanotubes have revealed good performance in detecting toxic gases and vapors of organic solvents. The latter sensors exhibited a fast response (e.g. 0.1 s) due to the presence of nitrogen sites, which are highly reactive. Therefore, it is possible to construct various types of nanotube composite pellets or circuits that are sensitive to gases and vapours, and that could be used to monitor leaks in chemical plants, thus saving numerous lives in various industries. Besides gas sensing, SWNTs could also be used as sensitive environment pressure sensors. In this context, Wood and co-workers noted that SWNTs are very sensitive to liquid immersion or polymer embedding because the nanotubes slightly deformed in the presence of different liquid media. Visible radiation and magnetic sensors could also be developed using carbon nanotube materials, however this work is currently under way. Very recently, the fabrication of gas ionisation sensors using films of pure and aligned carbon nanotubes was reported. This device consisted of a silver cathode and a MWNT anode, capable of monitoring the breakdown voltage of a specific gas, independent of humidity or temperature. These authors determined the gas quantities by measuring the current discharge of that specific gas. At present, this device is unable to detect low concentrations of gases because the interelectrode discharge is inhibited by other gases present in the mixture, such as air.

4. Gas and hydrogen storage

The inner hollow channel in carbon nanotubes (MWNTs and SWNTs) could be visualised as a container that could store various gases. Recent studies have revealed that hydrogen (H_2) and argon can be stored inside nanotubes. Argon could be introduced using high argon pressures for 48 h at 650˚C. Terrones et al. demonstrated that it is also possible to introduce gaseous nitrogen (N_2) inside MWNTs using a single step process: spray pyrolysis of $Fe(C_5H_5)_2$ (ferrocene) and $PhCH_2NH_2$ (benzylamine) solutions. Simultaneously, Trasobares et al. found similar results, but using powder pyrolysis of ferrocene– camphor under ammonia atmosphere. Many authors have emphasised that hydrogen (H_2) storage in carbon nanotubes may be advantageous in the fabrication of fuel cells mainly for powering electric vehicles. Unfortunately, there has been controversy regarding the high hydrogen storage capacity in carbon nanotubes (from 0.1 to 66 wt-%). More recent studies have indicated that the hydrogen uptake is lower than 2%, being the highest for HiPCo produced SWNTs. Hirscher et al. showed that the influence of impurities such as titanium (coming from the sonication probe) might be responsible for the results reported previously with uptakes up to 7%. From the theoretical point of view, density functional theory has been used to calculate the hydrogen (H_2) storage in SWNTs; however much lower values than those reported by Dillon et al. were found and alternative mechanisms whereby SWNTs adsorb hydrogen molecules were proposed (e.g. including chemisorption, adsorption at interstitial sites, and swelling of the nanotube array). At present, it seems that nanotubes may not be the best material for storing hydrogen, but additional experiments and further calculations should be carried out in order to clarify these results. The adsorption of other gases such as He, H_2, N_2, SF_6 in nanohorns, double-walled tubes, SWNTs, carbon foams has been recently achieved by Kaneko and co-workers.

5. Scanning probe tips

Multiwalled nanotubes have been successfully attached to scanning probe microscope (spm) silicon tips in order to enhance image resolution. The superior mechanical strength of carbon nanotubes and the facility to bend and recoil makes this material an excellent candidate for the production of long-life microscope tips. It is now possible to purchase MWNT scanning probe tips from Seiko Instruments and Daiken Chemical Company. Kim and Lieber have demonstrated that it is possible to fabricate nanotube tweezers by attaching two nanotubes on a probe tip. This nanotool operates by electrostatic interactions between the two carbon cylinders.

6. Nanotube electronic devices

Dekker and colleagues were the first to fabricate a three terminal switchable device based upon a single nanotube molecule. This transistor, operated at room temperature, and consisted of a semiconducting SWNT connected to metal nanoelectrodes. However, an inherent problem associated with nanotubes lies in the difficulty in manipulating them. In this context, another method devised to control the length and, consequently, the electronic properties of individual nanotubes by STM nanostructuring has been reported. Dekker's group also demonstrated that crossings and bends with SWNTs could be generated using an AFM. This technique allows one to cut nanotubes into shorter sections using controlled voltage applied at the STM tips, and to fabricate tiny nanotube devices that could be useful for future construction of molecular machinery and/or nanoscale circuits. As discussed above in the section 'Nanotube caps, helicoidal, toroidal and conical graphite', molecular junctions can also be created by inserting 5–7 defects. Experimentally, it was reported that metal–metal, metal–semiconductor, or semiconductor–semiconductor nanotube junctions could indeed be measured. In particular, the metal–semiconductor junction behaves like a rectifying diode with non-linear transport characteristics. It is believed that the controlled generation of such junctions will require further research using selfassembly growth processes.

More recently, Dekker and colleagues and Lieber and co-workers demonstrated the fabrication of field effect transistors (FETs), exhibiting favourable high gain, a large on-off ratio, and room temperature operation. The former group showed that one-, two-, and threetransistor circuits exhibit a range of digital logic operations, such as an inverter, a logic NOR, a static random access memory cell, and an ac ring oscillator. Similarly, Lieber's group produced crossed nanowire p–n junctions and junction arrays, that have been configured as key OR, AND, and NOR logic-gate structures with substantial gain, and could be used in the development of novel computer technologies. An IBM group, led by P. Avouris demonstrated that an individual SWNT can be used as a FET. The authors showed that SWNTs always behave as ptype transistors, whereas doped-nanotubes behave as ntype devices. Both types could then be integrated so that voltage inverters could be fabricated. A year later, Dai and co-workers confirmed that it is possible to generate logic rings as well as NOR, OR, NAND, and AND logic gates using arrays of p- and n-type nanotube FETs.

Since it is difficult to control the chirality of the tubes and thus the electronic properties, Collins et al. demonstrated that it is possible to peel outer layers of arc produced MWNTs until the desired electronic property of the outer shell is obtained. In a similar fashion, layers could be added to SWNTs so that the outer tubules meet the preferred electronic characteristics. However, recently, a group working in the USA431 succeeded in separating semiconductor and metallic SWNTs, using surfactants that were sensitive to semiconducting nanotubes. This results opens up new possibilities of developing SWNT devices based on assemblies of semiconducting and metallic nanotubes. Doped MWNTs can now be used as n and p type material so that novel p–n junctions and transistors can be created. It has been shown that nitrogen-doped carbon nanotubes behave as n-type nanowires, while boron-doped tubes act as p-type conductors. These results emphasise the importance of doping in the development of novel nanoscale electronic devices. In particular, these authors demonstrated that a temperature dependence in the thermoelectric power (TEP) of doped MWNT mats shows that nitrogen and boron dopants can be used to change the majority of carriers from p-type to n-type, in analogy with bulk semiconductors such as silicon. Specifically, at high temperatures the TEP of boron-doped nanotubes is large and positive, indicating hole-like carriers. In contrast, the

nitrogen-doped material shows a large negative TEP over the same temperature range, suggesting electronlike conduction. Although a tremendous amount of research has been carried out, further experiments need to be performed in the near future for assembling nanotubes into devices that could be launched onto the market. IBM experts envision that, in a decade, carbon nanotubes could be used in high performance electronic devices.

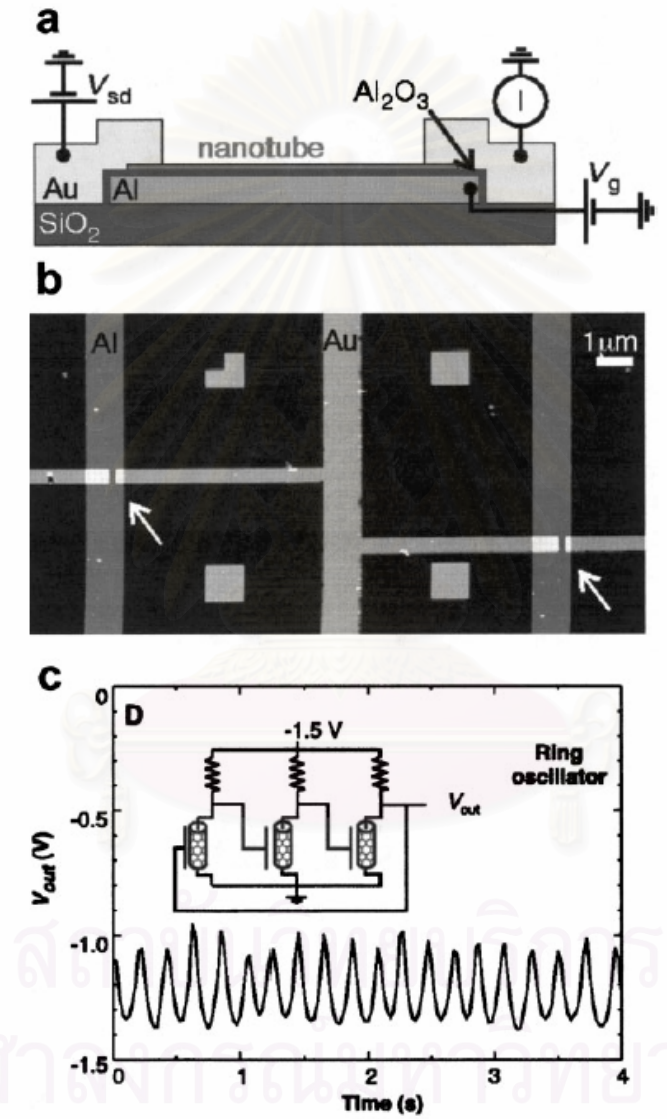

Figure 3 A schematic diagram of single-nanotube transistor

a) semiconducting SWNT is contacted by two Au electrodes, and an Al wire, covered by few-nanometres-thick oxide layer, is used as gate; b) height-mode AFM image of two nanotube transistors connected by Au interconnect wire (arrows indicate position of transistors); c) output voltage as function of time for nanotube ring oscillator (three resistances are 100 MV, 100 MV, and 2 GV),(courtesy C. Dekker)

APPENDIX D

Kinetics model of CNPs formation

Kinetics of CNPs formation

According to Lee et al. [16], the rate equation of CNTs could be assumed as zero order reaction (equation D.1). By employing the arrhenius equation one will be able to estimate the rate constant at any other temperature as shown in equation D.2.

$$r = kC^0 = k \tag{D1}$$

$$k = Ae^{-\frac{E_a}{RT}} \tag{D2}$$

Figure 1 illustrates the linear relationship between logarithm of rate of CNPs formation and $\frac{1}{T}$, of which slope is equal to $\frac{-E_a}{R}$ and interception of y axis is $\ln A$. Based on the obtained experimental results, rate of formation of carbon nanotube could provide the interception of 6.3 and the slope of 17.6×10^3.

Therefore, for carbon nanotubes formation, the rate equation can be expressed as shown in equation D.3.

$$r_{CNTs} = 992.27 \cdot e^{\frac{-146.5 \times 10^3}{RT}} \tag{D3}$$

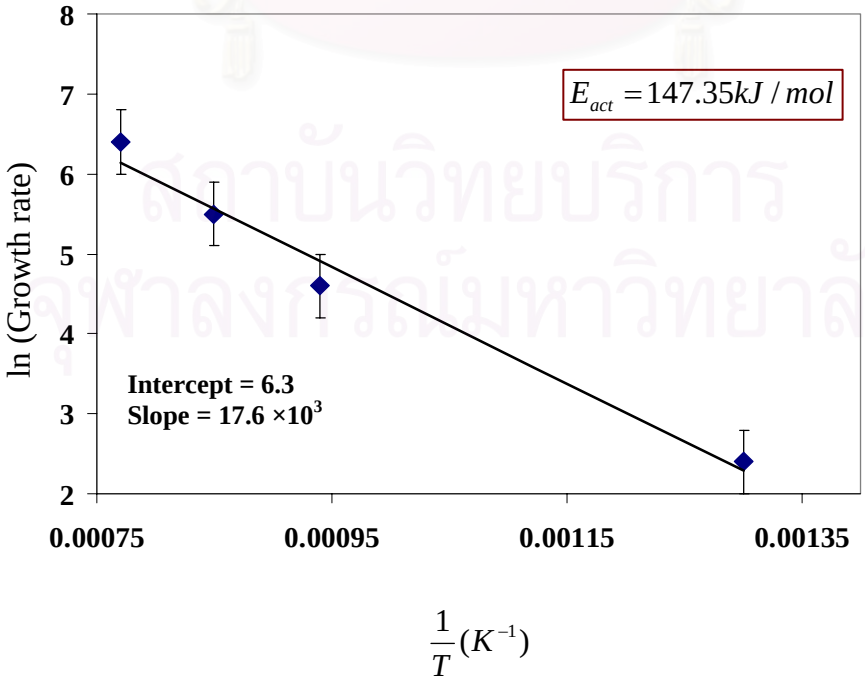

Figure 1 A typical Arrhenius plot for the growth rate of CNTs from Lee's experiment [23]

For rate of formation of CNCs, it could be assumed the same collision frequency (A value) with CNTs formation because both structures are carbon cluster. But CNCs has more similar structure with graphite structure compared with CNTs. Therefore, the activation energy of CNCs formation could be assumed from $\Delta H_{graphite}$ = 40.5 kJ/mol (equation D4-5 by assuming $\Delta S = 0$) which different from the activation energy proposed by Lee [23]. Similarly, for carbon nanocapsules, the rate equation obtained from experimental results is shown in equation D6.

$$\Delta G = \Delta H - T\Delta S = -RT \ln k \quad \text{(D4)}$$

$$\Delta H = -RT \ln k \quad \text{(D5)}$$

$$r_{CNCs} = 992.27 \cdot e^{\frac{-40.5\times10^{3}}{RT}} \quad \text{(D6)}$$

VITA

Mr. Pramote Puengjinda was born in Bangkok, Thailand, on April 5, 1981, the first son of Prayoon and Ausanee Puengjinda. After completing his high-school study at Wat Suthi Wararam school in Bangkok, in March 1999. He entered Chulalongkorn University, Bangkok, in June, 1999. After earning the degree of Bachelor of Engineering in Chemical Engineering in March, 2003, he gained admission to the Graduate School of Chulalongkorn University in June 2003. He received financial support from Thailand Research Fund, which covered research materials and monthly expenses. In April 2005, he was awarded the degree of Master of Engineering in Chemical Engineering.